

Case No. 5050/296

#13
4/21
RECEIVED

IN THE UNITED STATES PATENT AND TRADEMARK OFFICE

MAR 20 98
GROUP: 330

In re Application of:

Ted Christopher

Serial No: 08/746,360

Filed:

For: FINITE AMPLITUDE DISTORTION-
BASED INHOMOGENEOUS PULSE
ECHO ULTRASONIC IMAGING

Attn: Special Program Law
Office of the Office of
the Deputy Assistant
Commissioner for Patent
Policy and Projects

PETITION UNDER 37 C.F.R. § 1.292 FOR THE
INSTITUTION OF A PUBLIC USE PROCEEDING

Assistant Commissioner for Patents
Washington, D.C. 20231

RECEIVED

MAY 15 1998

Dear Sir:

Acuson Corporation (Acuson) hereby petitions for the institution of a public use proceeding to determine whether claims pending in the above-identified U.S. patent application (the "Christopher application") are patentable over the public uses described below.

OFFICE OF PETITIONS
DEPUTY ASST. COM. FOR PATENTS

The following materials are provided in support of this petition:

1. Two VHS videotapes labeled "Dr. Mulvahy Video II • Imaging" and "Mayo Clinic #CSI, Echo Date 9-28-94, Complete Copy" (collectively referred to as the "Mulvagh videotape");
2. a VHS videotape labeled "Contrast Echocardiography Investigations Copy A" (the "Acuson videotape");
3. evidentiary declarations of John M. Sheldon, Janna G. Clark, Paul E. Chandler, Sharon Mulvagh, M.D., Gregory L. Holley, and Joan C. Main;
4. a copy of form PTO-1449 listing the items of paragraphs 1-3;

04/03/1998 BALEXAND 00000060 08746360
01 FC:138

5. a check in the amount of \$1,510.00.

Additionally, Acuson hereby certifies that a duplicate copy of this petition, including all supporting materials, has been sent to RCT, the owner of the Christopher application by Federal Express on March 20, 1998, at the following address:

Mr. Timothy Reckart, Esq.
General Counsel, Secretary and
Director of Legal Affairs
Research Corporation Technologies
101 North Wilmot Road, Suite 500
Tucson, Arizona 85711-3335.

The supporting materials listed above provide evidence of two separate public uses, as follows:

The Acuson videotape shows recorded ultrasound images that were acquired using a fundamental transmit center frequency of 2.5 MHz (Chandler ¶ 3, Main ¶ 2) and a harmonic receive center frequency of 5.0 MHz (Chandler ¶ 3, Main ¶ 2). Selected portions of the images on the Acuson videotape show ultrasonic images of heart tissue obtained in the absence of contrast agent (Chandler ¶¶ 6-8, Holley ¶ 7, Main ¶¶ 14-15), and these images were generated at least in measurable part as a result of second harmonic distortion that occurs as the transmitted ultrasound pulse propagates through the tissues of an animal subject. Such distortion is identified as "finite amplitude distortion" in Ted Christopher's January 1997 paper (Chandler ¶ 8, Holley ¶ 7). The Acuson videotape was publicly shown in the United States at the American College of Cardiology Scientific Sessions during the week of March 14, 1993 (Clark ¶ 2) and at the floor show at the American Society of Echocardiography in June of 1993 (Main ¶ 12). The enclosed Acuson videotape is an accurate copy of the original tape (Sheldon ¶¶ 4-5, Chandler ¶ 5 and Main ¶ 13).

Similarly, the Mulvagh videotape records a series of ultrasonic images that were acquired using a fundamental transmit center frequency of 2.5 MHz and a harmonic receive center frequency of 5.0 MHz (Chandler ¶ 3, Mulvagh ¶ 3, Holley ¶ 3, Main ¶ 6). Portions of the Mulvagh videotape show resulting


images obtained from a dog's beating heart in the absence of added contrast agent (Mulvagh ¶ 4, Holley ¶¶ 4-5, Main ¶¶ 4 and 7). These portions of the Mulvagh videotape include images generated at least in measurable part from second harmonic distortion of the transmitted pulse caused by propagation through the tissues of the animal (Holley ¶ 8). The unedited Mulvagh videotape was publicly shown in the United States on September 30, 1994 at an echocardiography conference entitled "Advances in Echocardiography: Contrast Echocardiography Perfusion Imaging" (Mulvagh ¶¶ 2 and 6, Main ¶¶ 5 and 8). The enclosed Mulvagh videotape is an accurate copy of the original (Mulvagh ¶ 5, Sheldon ¶¶ 2 and 3).

As pointed out briefly in the preceding paragraphs, the enclosed declarations are evidence that ultrasound images of heart tissue, acquired at the second harmonic of the fundamental transmission frequency in the absence of added contrast agent, were in public use in the United States in March of 1993, June of 1993 and September of 1994. These images included a measurable amount of tissue harmonic signal resulting from second harmonic distortion of the fundamental ultrasound beam as it propagated through the tissues of the animal subject. Acuson wishes to have this information considered during the examination of the above-identified Christopher patent application, and Acuson submits that a public use proceeding is the proper procedure. Acuson has not yet reviewed the claims of the above-identified Christopher patent application, and is therefore not in a position to assert whether or not these claims are patentable over the public uses described above. Petitioner has a potential interest in acquiring rights in any patent maturing from the above-identified Christopher application, and Petitioner therefore wishes to have the above-described public uses considered carefully by the Patent Office in determining whether to grant a patent on the Christopher application.

Petitioner requests that the Commissioner institute a public use proceeding to allow these issues to be considered.

Respectfully submitted,

ACUSON CORPORATION



William A. Webb

Registration No. 28,277

BRINKS HOFER GILSON & LIONE
P.O. BOX 10395
CHICAGO, IL 60610
(312) 321-4200

FORM PTO-1449 LIST OF PATENTS AND PUBLICATIONS FOR APPLICANT'S INFORMATION DISCLOSURE STATEMENT (use several sheets if necessary)	SERIAL NO.	CASE NO.
	08/746,360	5050/296
	FILING DATE	GROUP ART UNIT
APPLICANT(S): Ted Christopher		

EXAMINER INITIAL	OTHER ART (Including Author, Title, Date, Pertinent Pages, etc.)	
	A1	Two VHS videotapes labeled "Dr. Mulvahy Video Imaging" and "Mayo Clinic #CSI, Echo Date 9-28-94, Complete Copy"
	A2	A VHS videotape labeled "Contrast Echocardiography Investigations Copy A"
	A3	Evidentiary declaration of John M. Sheldon
	A4	Evidentiary declaration of Janna G. Clark
	A5	Evidentiary declaration of Paul E. Chandler
	A6	Evidentiary declaration of Sharon Mulvagh, M.D.
	A7	Evidentiary declaration of Gregory L. Holley
	A8	Evidentiary declaration of Joan C. Main

RECEIVED
 MAR 20 98
 GROUP: 330

EXAMINER	DATE CONSIDERED
----------	-----------------

EXAMINER: Initial if reference considered, whether or not citation is in conformance with MPEP 609;
 Draw line through citation if not in conformance and not considered. Include copy of this form with next
 communication to applicant.

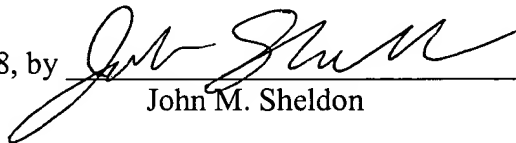
Evidentiary Declaration of John M. Sheldon

I, John M. Sheldon, declare the following facts to be correct based on my personal knowledge:

1. I have been employed at Acuson since 1989 as a photo/video technician. Accordingly, I am very familiar with videotapes and videotape copying.
2. I have reviewed the videotape with a thin crack in the right-hand window of the casing, referred to in Dr. Sharon Mulvagh's declaration. It is a VHS tape that has excerpts that were copied from the same Betacam tape from which I made four additional like excerpted copies on VHS tapes. Both the Betacam tape and the tape with the thin crack include a minor copying artifact that is symptomatic of Acuson's specific in-house copying set-up used when a Betacam copy is made from an original Super-VHS tape. I have placed my initials "JMS", and a copy *number* designation, on a label affixed to each of the four additional edited copies that I made.
3. In addition, I made three full (unedited) copies of the Betacam tape. I have placed my initials "JMS", and a copy *letter* designation, on a label affixed to each of the three additional unedited copies that I made.
4. I also made three VHS copies of an Acuson-produced S-VHS tape labeled "Contrast Echocardiography Investigations." I have placed my initials "JMS", and a copy *number* designation, on a label affixed to each of the three copies that I made.
5. Finally, I made an additional four VHS copies of the Acuson-produced Betacam tape from which the S-VHS tape referred to in paragraph 4 was made. The Betacam tape is labeled "Contrast Echocardiography Investigations Loop Copy," and the label bears a copyright notice (with Acuson's name mis-spelled) as follows: "Copyright 1993 Asuson". I have placed my initials "JMS" next to a copy *letter* designation on a handwritten label (entitled "Contrast Echocardiography Investigations") affixed to each of the four additional copies that I made.

I hereby declare under penalty of perjury that, to the best of my knowledge, the foregoing is true and correct.

Dated this 10th day of March, 1998, by


John M. Sheldon

RECEIVED
MAR 20 98
GROU 33

Evidentiary Declaration of Janna G. Clark

I, Janna G. Clark, declare that I believe the following facts to be correct based on my personal knowledge:

1. I have been employed by Acuson in clinical marketing/ sales support since March 1989.
2. In the 1992-1993 timeframe, I worked with Paul Chandler, who was the principal engineer investigating contrast imaging at Acuson. In late 1992 or early 1993, we took a model 128 Acuson ultrasound system to Dr. DeMaria, at the University of California at San Diego. At UCSD, under Dr. DeMaria's direction, we imaged Schering's contrast agent, Levovist, in a beating animal heart. I personally did some of the scanning for this imaging. We recorded the images on videotape, and then I edited the tape for presentation. We presented it to about 100 physicians and sonographers on Sunday March 14, 1993, which was the eve of the American College of Cardiology Scientific Sessions ("ACC"). In the following several days, during the ACC itself, I personally presented the videotape on the show floor. I kept the videotape running during show hours, and answered questions posed by conference attendees.

I hereby declare under penalty of perjury that the foregoing is, to the best of my knowledge, correct.

Dated this 10th day of March, 1998, by


Janna G. Clark

RECEIVED
MAR 20 1998
GRUP: 330

Evidentiary Declaration of Paul E. Chandler

I, Paul E. Chandler, declare that I believe the following facts to be correct based on my personal knowledge:

1. I was employed by Acuson as a Member of the Technical Staff from December 1986 to July 1994. I was a consultant to Acuson from May 1995 to November 1997. From July 1994 to May 1995, I was neither employed by nor consulting for Acuson, due to a disability. Since approximately 1991, a significant portion of my efforts were directed to my interest in the interplay between ultrasound systems and contrast agents.
2. In approximately 1992, at the suggestion of Reinhard Schlieff, I modified an Acuson 128 ultrasound system to support second harmonic imaging. This involved specifying the correct frequency pair to cause the system to transmit ultrasound energy at 2.5 MHz and receive ultrasound echoes at 5 MHz. To this end, I arranged to have the modification burned into a Programmable Array Logic (PAL) device on one of the boards, and I arranged to have the system software modified. I also procured a prototype wide band transducer from Acuson's Principal Fellow, Amin Hanafy. The whole process took a couple of days to complete.
3. This first system is called "Serial Number 1122" at Acuson. Subsequently, I instructed Art Tofanelli in how to modify other Acuson systems. In the next few years, pursuant to my requests and requests of others at Acuson, 8 additional systems were built in this manner. For all of these systems, when the 5.0MHz icon on the screen is highlighted, it means that the machine is configured to transmit ultrasound energy at a fundamental center frequency of 2.5MHz and receive ultrasound echoes from the anatomy and/or contrast agent at the second harmonic center frequency of 5MHz.
4. I worked with Joan Main, who led the Acuson marketing contrast effort. In late 1992 or early 1993, Ms. Main and a clinical marketing specialist, Janna Clark, accompanied me in taking Serial Number 1122 to Dr. DeMaria, at the University of California at San Diego. At UCSD, under Dr. DeMaria's direction, we imaged Schering's contrast agent, Levovist, in a beating animal heart. We recorded the images on videotape, and then the tape was edited for presentation to about 100 physicians at the ACC in 1993. I personally presented the edited videotape at the conference in a closed session.
5. Today, I reviewed Acuson's Betacam tape entitled "Contrast Echocardiography Investigations Loop Copy," which bears a copyright notice on the label (with Acuson's name mis-spelled) as follows: "Copyright 1993 Asuson". I have compared it to the S-VHS entitled "Contrast Echocardiography Investigations," which does not have the words "Loop Copy" or the copyright notice on the label. From this inspection, I am

RECEIVED
MAR 20 1998
FBI - LOS ANGELES

convinced that both tapes contain the same images and are copies of the original or copies of copies of the original, and that I showed one such tape at the ACC in 1993.

6. In conducting the experiments shown on the tape, we used a protocol that included looking at the heart tissue at the harmonic frequency in the absence of contrast agent, and then looking at the heart tissue after contrast agent was added. Accordingly, the videotape tapes created from the experiments displayed the images at the harmonic frequency both before and after contrast agent was added.
7. My purpose in running the experiments shown on the tape was to determine whether the second harmonic signals generated by the contrast agents could be seen above the signals at the second harmonic frequency known to be generated from the transmit pulse, the system nonlinearities, and the nonlinearities of the propagation path of the pulse through tissue.
8. I have read Ted Christopher's paper, "Finite Amplitude Distortion-Based Inhomogeneous Pulse Echo Ultrasonic Imaging," IEEE UFFC Vol. 44(1) January 1997. The harmonic images on the tape that I showed in 1993 were generated at least in part as the result of "finite amplitude distortion" as that term is used in Ted Christopher's publication. A copy of this publication is attached hereto.

I hereby declare under penalty of perjury that the foregoing is, to the best of my knowledge, correct.

Dated this 10th day of March, 1998, by


Paul E. Chandler

1 Reprint of Journal Article

Finite Amplitude Distortion-Based Inhomogeneous Pulse Echo Ultrasonic Imaging

Ted Christopher

Abstract—Ultrasonic pulse echo imaging in inhomogeneous media suffers from significant lateral and contrast resolution losses due to the defocusing effects of the inhomogeneities. The losses in lateral and contrast resolution are associated with increases in the width of the mainbeam and increases in sidelobe levels, respectively. These two forms of resolution loss represent significant hurdles to improving the clinical utility of biomedical ultrasonic imaging. A number of research efforts are currently under way to investigate the defocusing effects of tissue and to consider corrective measures. All of these efforts assume linear propagation, and base the image-formation process on the reception of the transmitted pulse. A novel pulse echo imaging scheme in which the image is formed using the finite amplitude distortion components of the received pulse is considered here. Alternatively, this could be described as image formation using the nonlinearly-generated higher harmonics.

In homogeneous beam propagations, it has been established that the sidelobes of nonlinearly-generated higher harmonics are much lower than their linear counterparts. Computations considered here suggest that this relationship also holds for the case of propagations through abdominal wall and breast wall tissue. These computations also suggest that the lateral resolution limits imposed by abdominal wall and breast wall tissue are slightly smaller for nonlinearly-generated second harmonics than for their linear counterparts. The resulting potential of these higher harmonics to improve image resolution is investigated.

I. INTRODUCTION

THE LOSS OF CONTRAST and lateral resolution due to phase aberrations produced by inhomogeneities in tissue is a significant problem in biomedical ultrasonic imaging [1]–[13]. A variety of phase aberration correction schemes have been considered [2], [5]–[7], [8], [10]–[11], [13]. These schemes have thus far demonstrated limited clinically-relevant success.

A new approach, and one independent of the existing approaches, involves using the finite amplitude or nonlinear distortion of the propagating beam to form an image. In this approach, the ultrasound image would be based on the received finite amplitude distortion components (or nonlinearly-generated higher harmonics) associated with the transmitted signal. In the simplest case in which the

transducer emits negligible energy in the second harmonic bandwidth, such an image could be formed by adding an initial high pass filtering of the received signal. In general, such an image could be formed by using a two pulse transmit, receive, normalize, and then high pass filtering scheme. Such a two pulse scheme could be used to remove the source or linear content in the second and higher harmonic bandwidths.

In the following section, the finite amplitude production of higher harmonic beams will be considered for the case of an apodized and focused Gaussian transducer operating in a non-aberrating liver medium. Both continuous and pulsed fields will be considered. The associated imaging-relevant sidelobe levels and mainbeam widths of the second and third harmonics will be considered there. In Section III, the requisite field amplitudes and their relationship to the proposed mechanical index (MI) will be considered.

In Section IV, the essential mathematics describing the formation of higher harmonic beams will be presented. This presentation provides insight into the homogeneous propagation results shown in Section II and a basis for understanding the subsequent inhomogeneous propagations considered. In Section V, inhomogeneities are added to the previously considered liver path propagation example. The inhomogeneities are in the form of planes of time delays, which were measured for abdominal wall and breast wall layers [4], [7]. Of particular interest in this section are the results depicting the relative impacts to the mainlobe widths and sidelobe levels of linear (fundamental) beams and nonlinear (higher harmonic) beams. Finally, in Section VI, the prospects for nonlinear imaging are discussed.

II. HOMOGENEOUS NONLINEAR PROPAGATION EXAMPLES AND ANALYSIS

A. Continuous Wave Sources

Several computational models exist which can accurately describe the finite amplitude propagation of a continuous beam. Such models can be extended to compute the case of a propagating pulse, as well. These models account for the effects of diffraction, nonlinearity, and absorption. The excellent accuracy possible with such models is depicted in [14]–[17]. The NLP model [16] was used to compute the following linear and nonlinear examples.

Manuscript received March 5, 1996; accepted July 22, 1996.

T. Christopher is with the Department of Electrical Engineering and Rochester Center for Biomedical Ultrasound, University of Rochester, Rochester, New York 14627 (e-mail: christo@ee.rochester.edu).

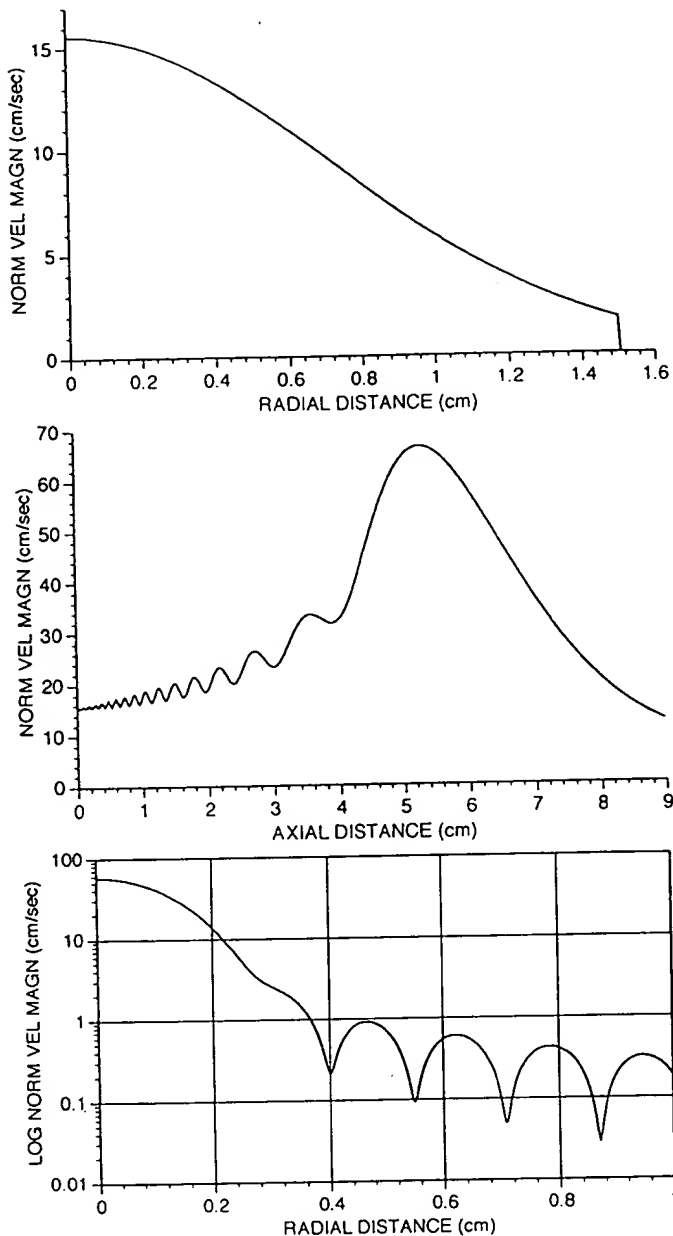


Fig. 1. Linear propagation results for a focused 2 MHz Gaussian transducer operating in a liver medium. (a) The source plane amplitude profile. (b) The on-axis amplitude. (c) The radial focal plane ($z = 6$ cm) beam profile.

This model has been updated to account for the effects of dispersion. The associated harmonic velocities were computed using a novel algorithm [18]. The NLP model also can account for the effects of refraction and reflection at a planar fluid boundary which, though not utilized in the following examples, could be relevant to modeling some *in vivo* propagations.

All of the following propagations are for a Gaussian apodized, axially symmetric focused source. This form of device should offer excellent image quality and produces a field comparable to the two-dimensional array-based transducers now being developed. The phase aberrated fields of these devices, considered in Section V, were not ax-

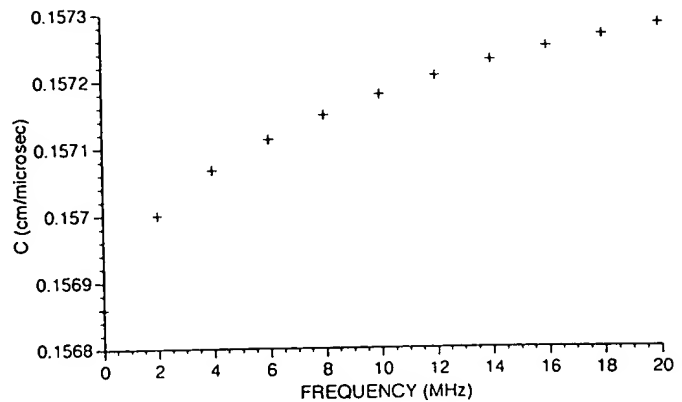


Fig. 2. The harmonic velocities used in propagating the 2 MHz Gaussian beam through liver.

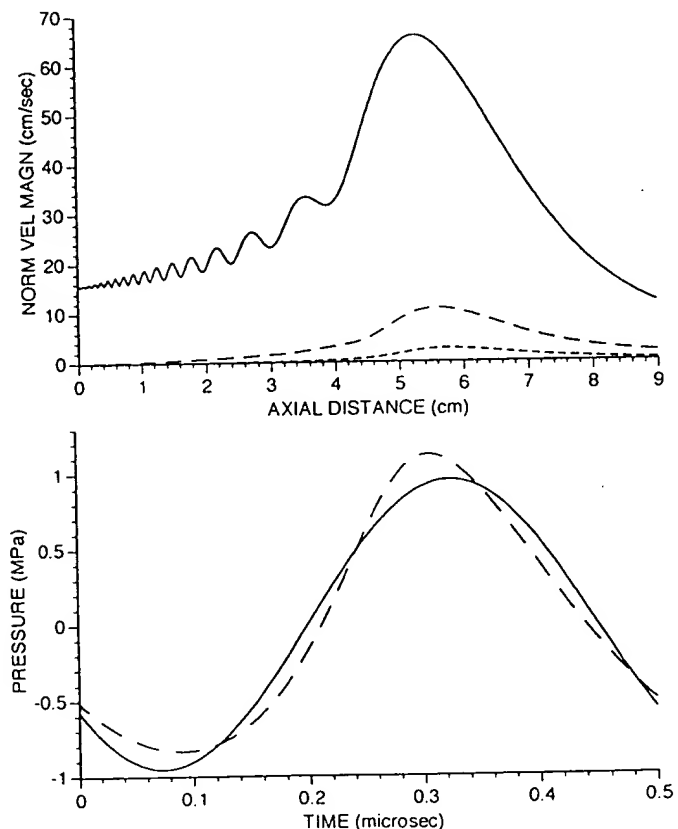


Fig. 3. Nonlinear propagation results for the focused 2 MHz Gaussian transducer. The propagation medium here and in all subsequent figures is liver. (a) The on-axis amplitudes of the fundamental, second, and third harmonics (top to bottom curves, respectively). (b) The focal ($z = 6$ cm) linear (solid curve) and nonlinear (dashed curve) waveforms.

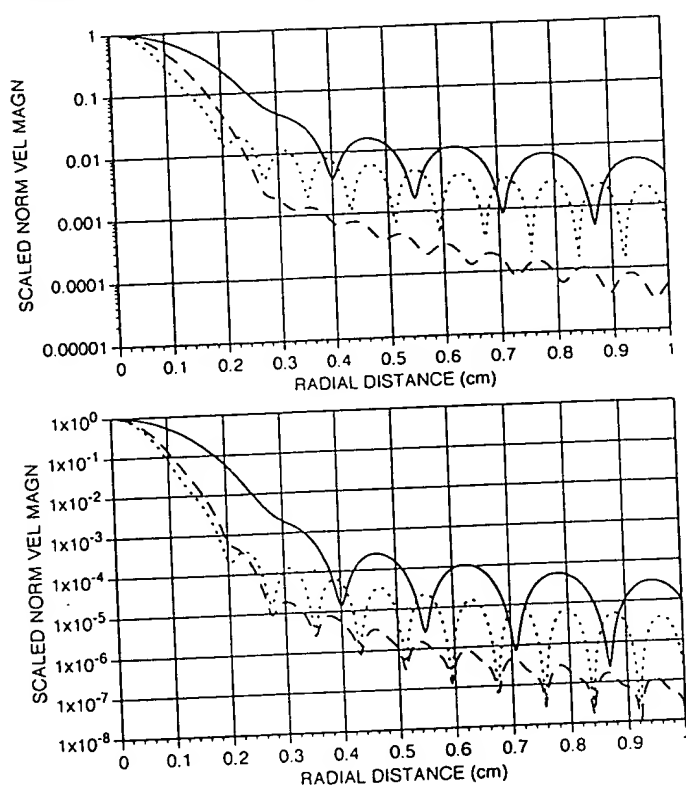


Fig. 4. Fundamental and second harmonic, one- and two-way focal plane beam patterns. (a) The log-scaled, normalized one-way focal plane profiles of the 2 MHz fundamental (solid curve), the 4 MHz second harmonic (long dash curve), and the 4 MHz fundamental (short dash curve). (b) The corresponding two-way profiles.

ially symmetric. In order to model these fields a two-dimensional version of NLP was utilized.

Many biomedical imaging devices are not axially symmetric, though. The finite amplitude beams produced by such devices should be well described by the computations for the axially symmetric transducer considered here. In measuring the nonlinear harmonic generation from an unfocused rectangular source, Kamakura, Tani, Kumamoto, and Ueda [19] noted that "the [nonlinear] harmonic pressure levels in the far field [were] almost the same as from a circular aperture source with equal face area and equal initial pressure, independent of the source levels." Though this result was obtained for only one device (with a ratio of source side lengths or aspect ratio of 11 to 6) it should be the case that the higher harmonic pressure levels associated with a non-axially symmetric device should be approximately equal to those of the corresponding axially symmetric source. More importantly, the lack of axial symmetry should not affect the relative sidelobe advantages exhibited by the nonlinearly-generated harmonics in a homogeneous propagation. Experimental results [20] support this point. These homogeneous path sidelobe level advantages are the basis for the imaging-relevant advantages in an inhomogeneous propagation. The results displayed in Fig. 1 were obtained by computing the linear, liver path propagation of the field of a focused 2 MHz Gaussian source using the NLP beam propagation model.

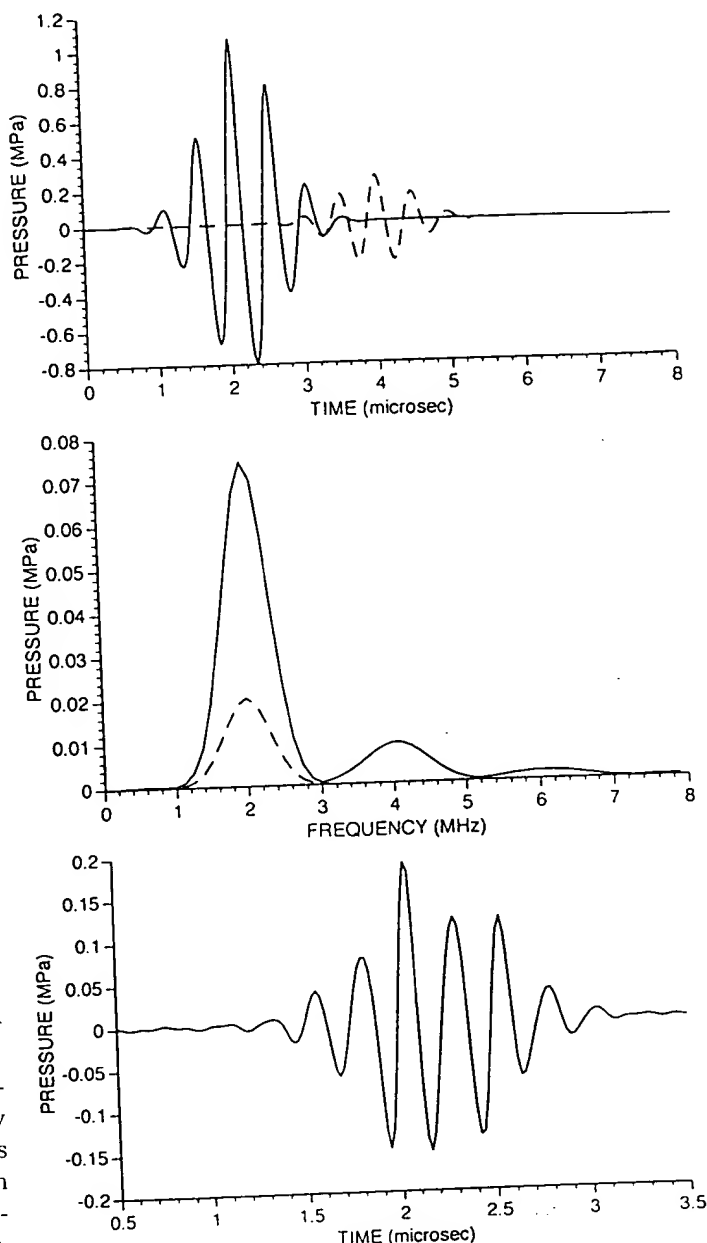


Fig. 5. (a) The on-axis source plane (dashed curve) and subsequent focal plane (solid curve) 2 MHz-centered pulses. The period of the pulses is 8 microseconds. (b) The corresponding spectra. (c) The focal nonlinear distortion pulse obtained by constructing the waveform using only the focal spectral information shown in (b) from 3 to 8 MHz.

The NLP model propagates a planar, normal velocity description of the acoustic field. No inhomogeneities or phase aberrations were accounted for in this propagation or any of the subsequent propagations considered in this section. The relevant liver propagation parameters used were $c = 1570$ m/s, $\rho = 1.05$ g/cm³, $\alpha = 0.03$ Np/cm, and $b = 1.3$ (where α and b are the coefficients describing absorption in a power law form) [21],[22].

The Gaussian amplitude shading of the source plane, normal velocity field was such that the half-amplitude radial distance was 0.84 cm. The on-axis, source plane RMS

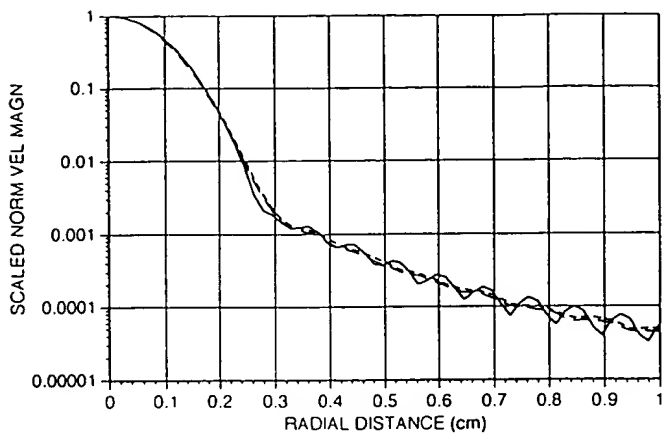


Fig. 6. Focal plane profiles from the 2 MHz continuous wave propagation (of Section II.A.) and the 2 MHz-centered pulse propagation (of Section II.B.). The solid curve depicts the 4 MHz second harmonic profile. The long dashed curve depicts the temporal peak amplitude profile computed using the frequency bandwidth of 3 to 8 MHz. The short dashed curve depicts the corresponding peak amplitude profile for the frequency range of 3 to 5 MHz.

acoustic intensity ($\rho c|u|^2/2$, where u is the acoustic particle velocity) for this field was 2 W/cm^2 . The radial extent of the source was 1.5 cm. The source plane field was focused using a spherically-focusing factor ($e^{j\theta(r)}$, where $\theta(r) = (2\pi f/c)\sqrt{r^2 + F^2}$). The geometric focal length F was 6 cm and the sound speed (c) used to compute $\theta(r)$ was that of water (1500 m/s).

Figs. 1a and (b) depict the normal velocity magnitudes of the Gaussian transducer's source plane and on-axis fields, respectively. Fig. 1c displays the focal plane ($z = 6 \text{ cm}$) radial profile of the 2 MHz field. The drop in the magnitude of the field from the mainlobe to the first side-lobe in Fig. 1c is 36 dB. In the absence of strong medium phase aberration, this should allow the device to produce high contrast images.

The same 2 MHz Gaussian source was then propagated nonlinearly through the same liver path. The nonlinear parameter β used to represent liver was 4.7 [23]. The NLP model used 4 harmonics (2, 4, 6, and 8 MHz) to compute the pre-focal region ($z = 0$ to $z = 3 \text{ cm}$) propagation and up to 10 harmonics to represent the subsequent focal and post-focal region propagation. The harmonic velocities were computed using a novel algorithm described in [18]. The fundamental or 2 MHz component had a propagation speed of 0.157 cm/microsecond (given above as c). The discrete harmonic velocities used by NLP to compute the 2 MHz propagation are shown in Fig. 2.

Fig. 3a displays the axial magnitudes of the fundamental, second harmonic, and third harmonic fields as computed for the nonlinear propagation. The fundamental or 2 MHz axial curve is only slightly different from the corresponding linear curve shown in Fig. 1b. At $z = 6 \text{ cm}$, the nonlinear 2 MHz curve is about 1% lower than the 2 MHz linear curve. This difference was due to growth of the higher harmonics in the nonlinear propagation. In Fig. 3b the corresponding focal ($z = 6 \text{ cm}$) pressure waveforms

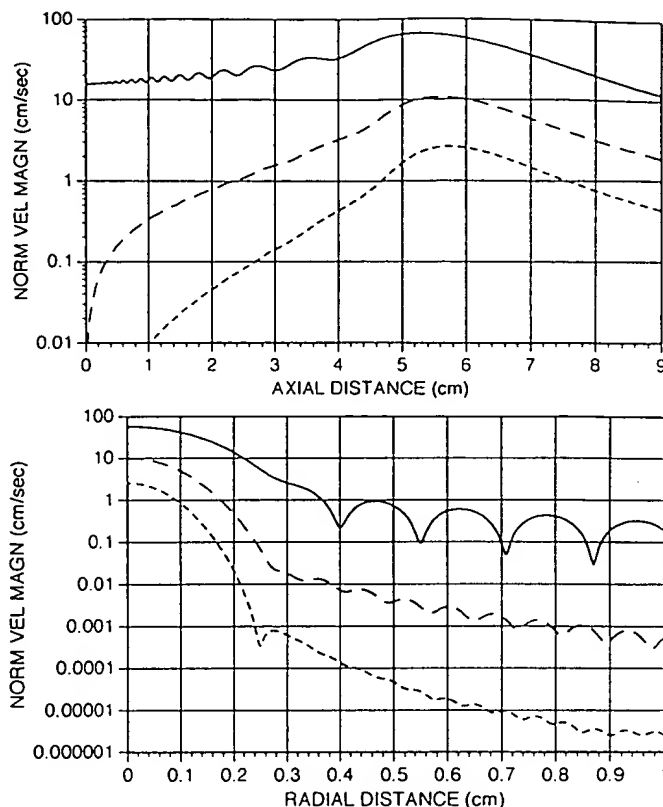


Fig. 7. (a) Log-scaled first, second, and third harmonic axial amplitudes (top to bottom, respectively) for the focused 2 MHz Gaussian transducer. (b) The corresponding log-scaled, focal plane radial beam profiles.

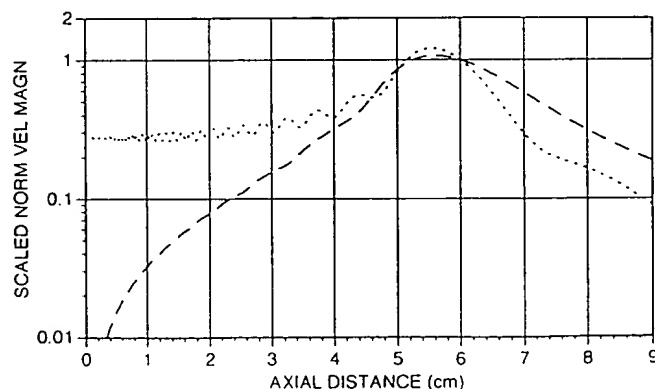


Fig. 8. Log-scaled axial amplitudes for the 4 MHz second harmonic and 4 MHz fundamental harmonic beams. The amplitude curves have been normalized to have equal 1.0 at $z = 6 \text{ cm}$. The long dash curve represents the second harmonic.

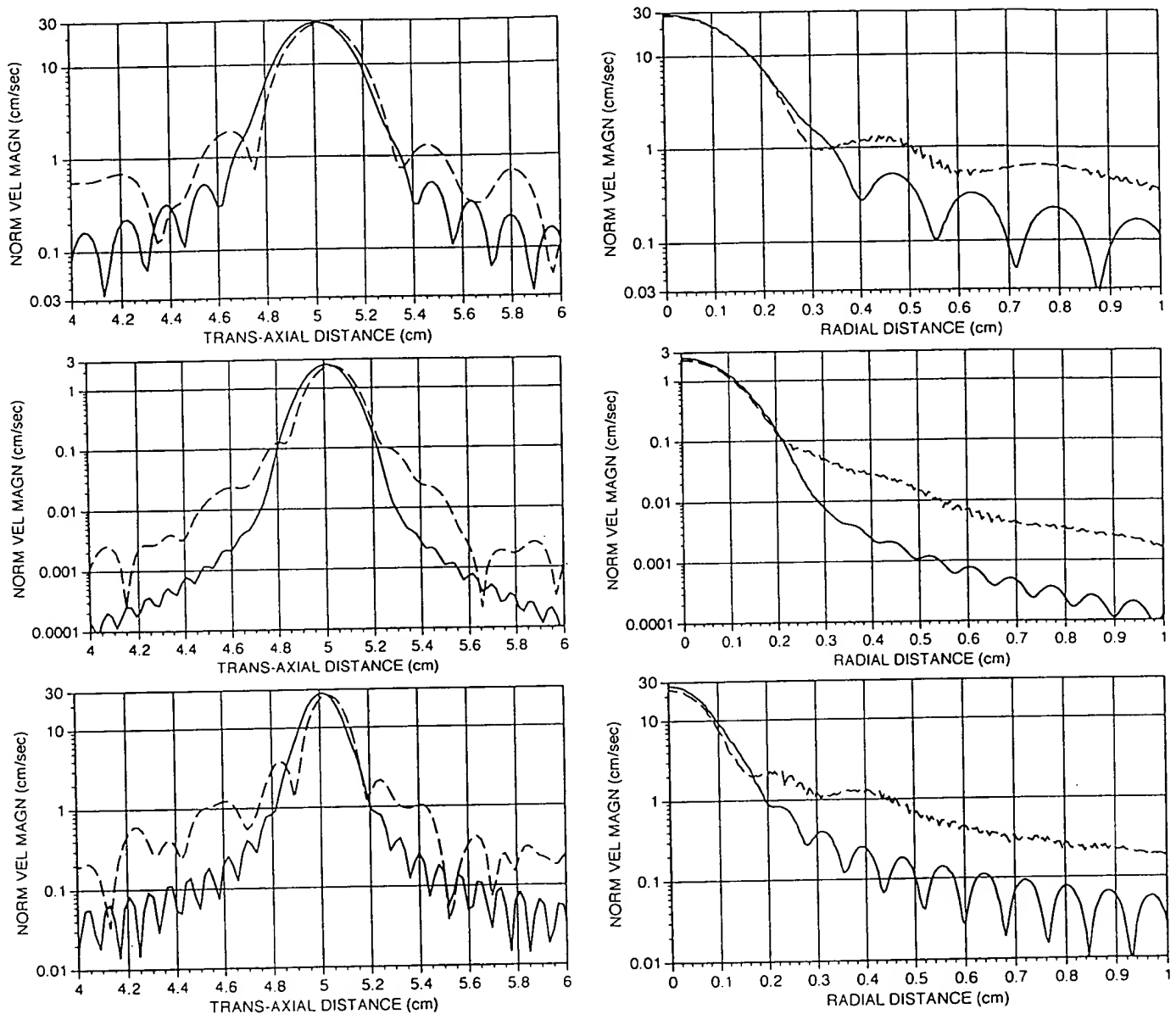


Fig. 9. Homogenous and abdominal wall-jittered tissue path beam propagation results for the 2 and 4 MHz focused Gaussian transducers. Focal plane (one-way) profiles. the solid curves are the un-jittered or homogeneous tissue path results. (a) 2 MHz fundamental diameters. (b) Average radii from the 2 MHz focal plane profiles. (c) 4 MHz second harmonic diameters. (d) Average radii from the second harmonic 4 MHz profiles. (e) and (f) same format for the 4 MHz fundamental profiles.

are displayed. The pressure waveforms were obtained by converting NLP's normal velocity output to pressure using the impedance relation (all subsequent pressure waveforms were obtained in this way).

The 2 MHz or fundamental beam pattern associated with the nonlinear propagation is almost identical with the 2 MHz beam pattern of the linear propagation. Only in a linearly scaled overlay plot of the two beam patterns are there visible differences. These differences are very small and are limited to the near axis portions of the beam patterns. Only at much higher source intensities [16],[24] are the effects of nonlinearity significant to the details of the fundamental's field. These results are consistent with the empirical observation that linear modeling of biomedical

ultrasonic device fields accurately describes their (linear-based, homogeneous path) imaging performance.

Fig. 4a depicts the 2 MHz fundamental and 4 MHz second harmonic focal plane amplitude profiles. Also shown in Fig. 4a is the corresponding 4 MHz fundamental profile. The 4 MHz fundamental result was obtained by computing the linear propagation of the same Gaussian transducer operating at a source frequency of 4 MHz. All three beam profiles have been normalized to have on-axis field amplitudes of 1. The finite amplitude distortion-generated second harmonic focal profile has a slightly broader main-lobe than the corresponding (4 MHz) fundamental profile. The radial half-amplitude distance of the second harmonic profile is 36% greater than that of the 4 MHz fundamental

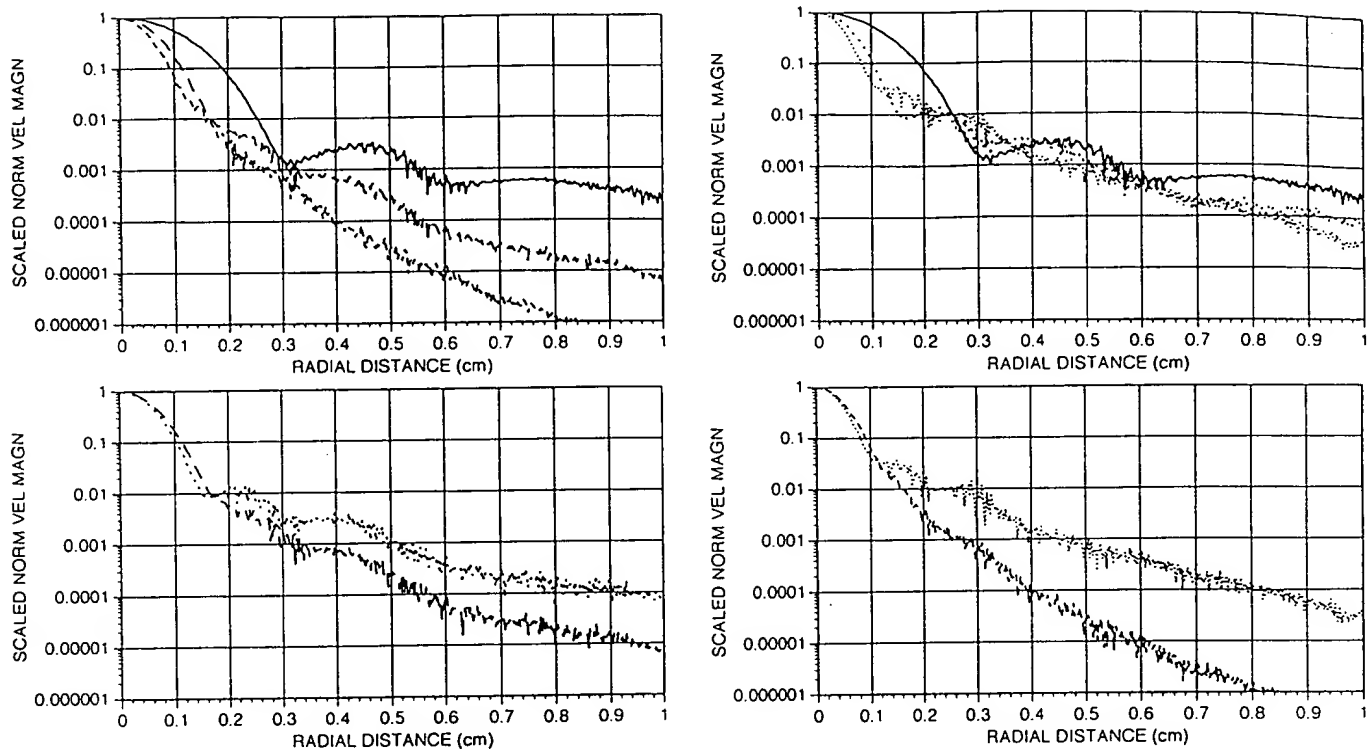


Fig. 10. Additional results from the abdominal wall-jittered propagation path case shown in Fig. 9. (a) 2 MHz fundamental, 4 MHz second harmonic, and 6 MHz third harmonic average two-way radii. (b) 2 MHz, 4 MHz, and 6 MHz fundamental or linear average two-way radii. (c) 4 MHz second harmonic and fundamental average two-way radii. (d) 6 MHz third harmonic and fundamental average two-way radii. The 4 and 6 MHz fundamental results in (c) and (d) are the shorter dash curves.

profile (0.0983 cm versus 0.0723 cm). The second harmonic profile also has much lower sidelobes than the 4 MHz fundamental profile.

For imaging purposes, the two-way focal plane beam pattern of the Gaussian transducer is of interest. The two-way focal beam pattern should account for both the characteristics of the transmitted pulse in the focal plane and the corresponding sensitivity of the transducer to pulses reflected back from this plane. For linear propagations, the two-way beam pattern for a given depth can be obtained by squaring the corresponding transmit or one-way beam pattern. Fig. 4b depicts the normalized two-way linear beam patterns for the Gaussian transducer operating at 2 and 4 MHz. These curves were obtained by squaring the corresponding one-way or transmit beam patterns shown in Fig. 4a.

Also shown in Fig. 4b is the two-way focal plane beam pattern associated with the 4 MHz second harmonic field. Since the amplitudes of the reflected pulses are much smaller than the transmitted pulses, the propagation of the reflected field back to the transducer is essentially linear. Thus the two-way, second harmonic focal plane beam pattern was obtained by multiplying the corresponding one-way pattern shown in Fig. 4a by the 4 MHz fundamental one-way pattern also shown in Fig. 4a.

The second harmonic's two-way beam pattern has a half-amplitude mainlobe width (or -6 dB beamwidth) that is 12% greater than that of the corresponding fun-

damental beam pattern. The -20 dB beamwidth of the second harmonic is 13% greater than that of the 4 MHz fundamental. The sidelobe advantage displayed in the focal plane profiles of Fig. 4a is maintained in the two-way results of Fig. 4b.

These homogeneous liver path results suggest that the second harmonic field of a focused, apodized transducer might offer advantages in contrast resolution over the corresponding or same-frequency transducer field. The results also suggest that these advantages would be slightly offset by losses in lateral resolution.

B. Pulse Sources

A pulse propagation was next considered for the 2 MHz Gaussian source. The on-axis, source plane pressure pulse used is displayed in Fig. 5a as the dashed curve. This pulse was computed by applying a Gaussian window to a 2 MHz cosine. The peak pressure of the pulse was the same as for the 2 W/cm^2 continuous case considered in Section II.A. The apodization and the spherical focusing of the source field were also the same as in the previous continuous wave case. The initial source plane pulse consisted of 128 samples across 8 microseconds.

The magnitude of the Fourier transform of the 8-microsecond source pulse is shown in Fig. 5b. A straightforward implementation of the nonlinear imaging idea requires that there be negligible overlap between the source's spectral bandwidth and that of the nonlinear second har-

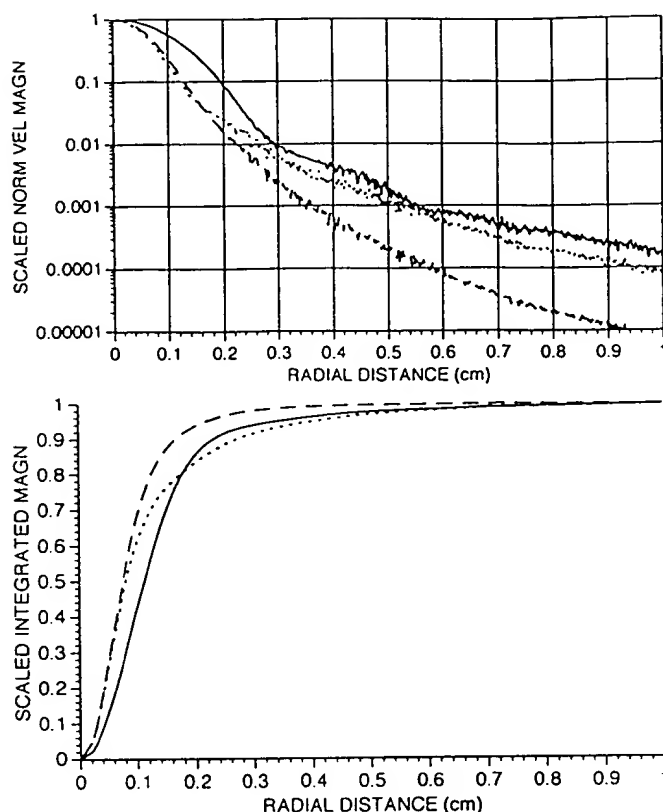


Fig. 11. Two-way averaged radial results from five abdominal wall-jittered propagations. (a) Normalized two-way average radii for the 2 MHz fundamentals (solid curve), 4 MHz second harmonics (long dash curve), and 4 MHz fundamentals (short dash curve). (b) The corresponding radially integrated magnitudes. These curves have been normalized to have a unity value at $r = 1.2$ cm.

monic. (More generally, this would also insure negligible overlap between any of the successive harmonic spectral bands.) The source spectrum shown in Fig. 5b meets this requirement. Nonlinear images based on source pulses with broader spectrums or with significantly more energy in the second harmonic bandwidth than the one depicted in Fig. 5 could be obtained by using an alternative nonlinear imaging scheme described in Section VI.

The source plane was then defined using the 64 harmonic Fourier transform of the source pulses. This multi-harmonic source radius was then input into a pulse-propagating version of the NLP model (a model similar to the lithotripter model [25]). The focal output of the resulting nonlinear pulse propagation is also shown in Fig. 5a and 5b as solid curves. The focal pulse waveform has slightly smaller peak positive and negative pressures than the corresponding continuous waveform shown in Fig. 3b. Consistent with the smaller amplitudes, the focal pulse is also less distorted than the continuous waveform. The ratio of the second harmonic's focal amplitude to that of the fundamental's for this pulse propagation was 70% of the same ratio for the corresponding continuous source considered in Section II.A.

Fig. 5c shows the waveform associated with only the spectral bands of the second, third, and the first half of the

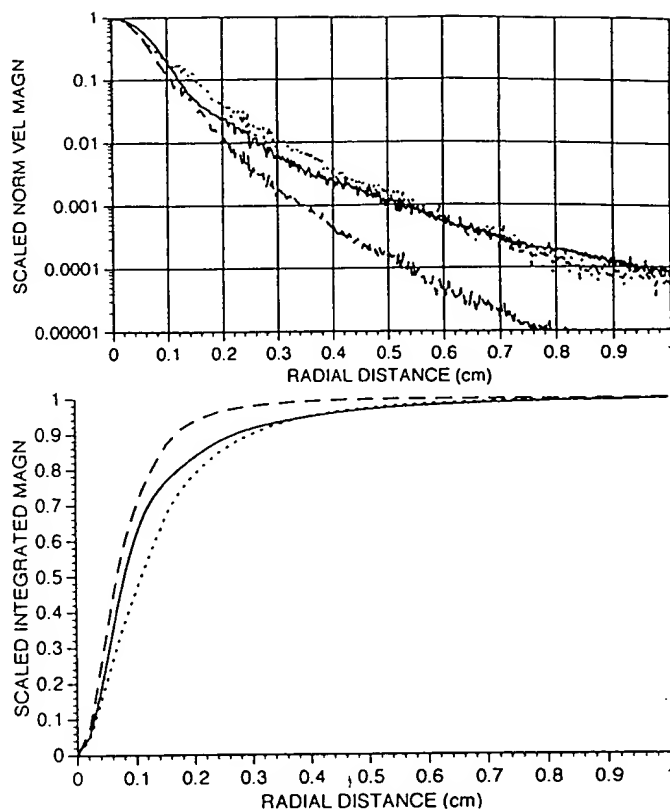


Fig. 12. Two-way averaged radial results from five abdominal wall-jittered propagations. (a) Normalized two-way average radii for the 4 MHz fundamentals (solid curve), 8 MHz second harmonics (long dash curve), and 8 MHz fundamentals (short dash curve). (b) The corresponding radially integrated, normalized magnitudes.

fourth harmonic (3 through 8 MHz). This waveform was computed as a high pass filtered reconstruction of the spectral information depicted in Fig. 5b. A rectangular window with a transition at 3 MHz was used in filtering the transform data. The straightforward nonlinear imaging approach considered here would use a distortion pulse like that shown in Fig. 5c in order to image the scattering medium.

Not shown for the pulse propagation considered are the axial and radial harmonic descriptions. These descriptions were found to be identical in form to those computed for the nonlinear propagation of the continuous 2 MHz field. All other Gaussian-windowed cosine pulses were found to produce identical axial and radial harmonic patterns.

The temporal peak amplitude profile of the high pass filtered-focal plane data also very closely followed the form of the 4 MHz second harmonic's amplitude profile. The temporal peak amplitude profile for the pulse propagation considered in this section is shown in Fig. 6. This profile was computed using the focal plane frequency data in the range of 3 to 8 MHz (like the waveform in Fig. 5c). Also shown in Fig. 6 are the corresponding 4 MHz second harmonic profile and a second harmonic bandpass filtered (3 to 5 MHz)-temporal peak amplitude profile for the same pulse propagation. The similarity of the two peak amplitude profiles suggests that there is very little energy above 5 MHz for this pulse propagation.

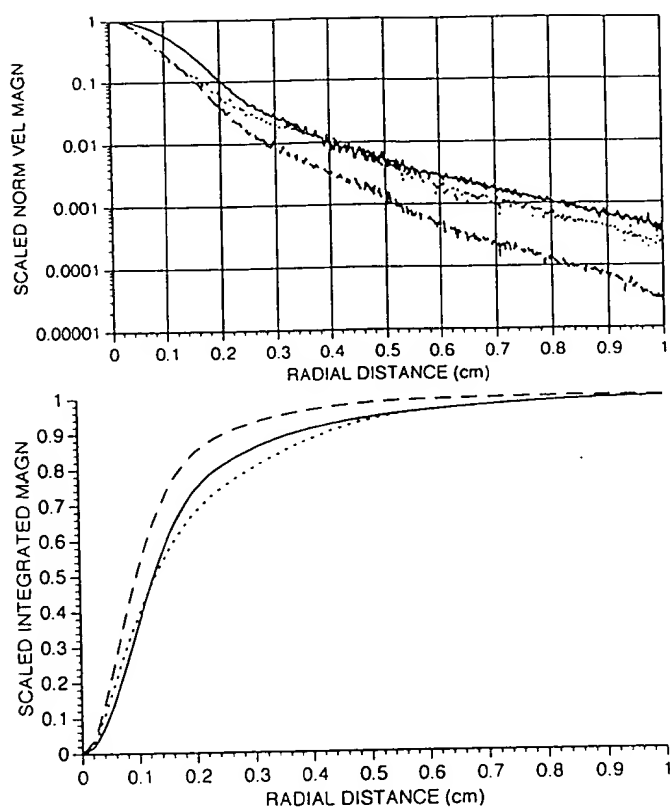


Fig. 13. Two-way averaged radial results from five breast-jittered propagations. (a) Normalized two-way average radii for the 2 MHz fundamentals (solid curve), 4 MHz second harmonics (long dash curve), and 4 MHz fundamentals (short dash curve). (b) The corresponding radially integrated magnitudes. These curves have been normalized to have a unity value at $r = 1.2$ cm.

As shown for the second harmonic bandwidth in this case, it appears that the higher harmonic peak amplitude patterns produced by any reasonable source pulse can be computed using an appropriate continuous approximation of the source. This is a very convenient relationship.

III. REQUISITE FIELD AMPLITUDES

In order for the nonlinearly-generated higher harmonics to be available for imaging in an inhomogeneous media, the received higher harmonics amplitudes can't be too low relative to the received linear (or transmitted) signal and the receiver's dynamic range. Also, to be available for imaging use, the associated *in vivo* field amplitudes must not correspond to a mechanical index greater than 1.9.

For the previously considered 2 MHz liver-path propagation, the amplitudes at the focus ($z = 6$ cm) of the fundamental and second harmonic were 0.943 MPa and 0.166 MPa, respectively. The second harmonic amplitude was thus 15.09 dB below the amplitude of the 2 MHz transmitted wave. As a wave reflected at the focal point travels the 6 cm back to the transducer/receiver, frequency dependent attenuation reduces the second harmonic by an additional 5.62 dB relative to the 2 MHz component. The

received 4 MHz component would thus be 20.71 dB below the transmitted 2 MHz component. (Ignored here is the possible additional relative weakening of the second harmonic received signal due to coherent reflectors at the focus in combination with the smaller mainlobe of the second harmonic. This effect should not be significant to many bio-ultrasound imaging applications, though.) The corresponding figures for the 6 MHz third harmonic were 27 dB down at the focus and 39.23 dB down for received signals.

Table I displays the second and third harmonic received levels corresponding to on-axis, source plane intensity values of 0.5, 1, 2, 4, and 8 W/cm². For a given source plane intensity, pulsed devices would have slightly larger received level differentials than those shown in Table I. For the pulsed propagation considered in the previous section, this additional gap would be 0.86 dB for the second harmonic (based on a second harmonic bandpass reconstruction and a comparison of the received peak positive pressure levels).

Current biomedical ultrasonic imaging transducers have dynamic ranges of about 100 dB. Even with decreased sensitivity above the transmit frequencies, these devices may be capable of creating second harmonic images. This capability may well have been demonstrated by the creation of second harmonic contrast agent-response images. Alternatively, a separate receiver device with appropriate frequency response in the desired nonlinear distortion bandwidth could be used.

The effect of focal length on the received second harmonic levels for this Gaussian transducer operating at 2 W/cm² is shown in Table II. From a focal length of 4 cm up to a focal length of 12 cm, the received second harmonic levels dropped off by 7.32 dB. Also shown in Table II are the corresponding focal second harmonic levels. These levels remained very constant and thus revealed the decreases in received levels as almost entirely due to increased return trip distances.

The peak positive and negative pressures of the predicted *in vivo* nonlinear waveform shown in Fig. 3b were 1.12 and -0.84 MPa, respectively. The -0.84 peak rarefaction pressure corresponds to a mechanical index (MI) of 0.59. The highest acceptable level for the mechanical index is 1.9. Shown in Table I are values of the minimum focal pressure and associated mechanical index for this and four other values of source plane intensity. Note that the minimum pressures and thus mechanical indices given in Table I have been corrected for the effects of nonlinearity. A linear-only computation would have predicted larger negative pressures and MI values, in particular at the highest two source intensity levels.

The numbers shown in Table I suggest that for *in vivo* propagations similar to the one considered here, finite amplitude distortion-based images should be readily obtainable within the current mechanical index safety limit. Even at the lowest source intensity case considered (0.5 W/cm²), a largely second harmonic-based image could be obtained by simply filtering out the transmitted frequency(ies). Additionally, the second and third harmonic received levels could offer some real-time feedback on the magnitude of

TABLE I
ON-AXIS (SPATIAL PEAK) SOURCE PLANE INTENSITY VERSUS RECEIVED SECOND AND THIRD HARMONIC LEVELS
(RELATIVE TO 2 MHz FUNDAMENTAL) AND FOCAL FIELD PARAMETERS.

On-axis source intensity (RMS w/cm^2)	Received 2nd harmonic level (dB)	Received 3rd harmonic level (dB)	Minimum pressure at the geometric focus (MPa)	Mechanical index $\left(\frac{\text{min. press.}}{\sqrt{f}}\right)$
0.5	26.54	50.88	-0.45	0.32
1	23.64	45.02	-0.61	0.43
2	20.73	39.23	-0.84	0.59
4	17.94	33.66	-1.13	0.80
8	15.37	28.59	-1.50	1.06

the focal field amplitudes themselves. Finally, the results displayed in Table II suggest that second harmonic imaging may be available at a wide range of focal depths.

IV. BASICS OF NONLINEAR BEAM FORMATION

The formation of the higher harmonic constituent beams in a propagating finite amplitude beam is a continuous process. In the case of the 2 MHz Gaussian-shaded, focused beam considered thus far, the 4 MHz second harmonic, the 6 MHz third harmonic, and additional higher harmonics are continuously and cumulatively produced by the beam as it propagates away from the source. Of interest here is the production and focusing of these nonlinear higher harmonic beams between the source and focal plane.

The origin of the higher harmonic beams is the ongoing nonlinear distortion of the propagating waves comprising the (total harmonic) focused beam. The physical effects of diffraction and absorption concurrently act on the higher harmonic beams and thus further define their propagation as well as contribute to changes in the resulting focused beam. The NLP model assumes that the nonlinear or finite amplitude distortion acts in a plane wave fashion on the waves comprising the focused beam [16]. The NLP model uses the frequency domain solution to Burgers' equation in an incremental Δz fashion to account for this plane wave distortion approximation. (See [16] for further details including the inclusion of the local directionality of the beam front, which is neglected in the following presentation.)

The frequency domain solution to Burgers' equation as used in the NLP model can be written

$$\frac{\partial u_n}{\partial z} = j \frac{\beta \pi f}{2c^2} \left(\sum_{k=1}^{n-1} k u_k u_{n-k} + \sum_{k=n}^N n u_k u_{k-n}^* \right),$$

$$n = 1, 2, \dots, N, \quad (1)$$

where f is the fundamental frequency and u_n is the n th term in an N term complex Fourier series describing the temporal normal velocity waveform at a point in the radial description of the field. The first summation term in the parentheses represents the accretion of the n th harmonic by nonlinear combination of other harmonics that have a

TABLE II
FOCAL AND RECEIVED SECOND HARMONIC LEVELS (RELATIVE TO THE FUNDAMENTAL) VERSUS FOCAL LENGTH. THE GEOMETRIC FOCUS OF THE 2 MHz GAUSSIAN TRANSDUCER AND THE PROPAGATION LENGTH OF THE MODEL WERE SET TO THE FIVE DISTANCES (6 CM IN THE PREVIOUSLY CONSIDERED CASE). THE ON-AXIS SOURCE INTENSITY WAS 2 W/CM² FOR ALL OF THE PROPAGATIONS.

Focal length (cm)	2nd harmonic level at the focus (dB)	Received 2nd harmonic level (dB)
4	15.99	19.75
6	15.11	20.73
8	15.01	22.53
10	15.29	24.69
12	15.83	27.07

sum frequency of nf . The second summation term (with conjugation) represents the depletion of the n th harmonic to other harmonics with a difference frequency of nf . For the case of a Fourier representation of a (periodic) pulse waveform, this accretion and depletion of harmonics results in some interesting phenomenon, including the production of a distortion bandwidth below the fundamental bandwidth.

Of interest to the results presented in this paper are the terms in (1) contributing to the growth of the second harmonic and, to a lesser extent, the third harmonic. When n equals 2 in (1) the positive contributions to $\frac{\partial u_2}{\partial z}$ come from the $1u_1u_1$ term comprising the first summation. The negative contributions to the second harmonic are represented by the second summation in (1) and, for the propagations under consideration here, can be approximated by the second term in that summation, $2u_3u_1^*$. Even this term, though, is negligible throughout most of the source to focal region propagation due to the relatively small amplitudes of the third harmonic. Thus, the nonlinear production of the second harmonic throughout most of the relevant propagation region is simply proportional to the square of the amplitude of the fundamental.

When n equals 3 in (1), the positive contributions to $\frac{\partial u_3}{\partial z}$ come from the first two terms comprising the first summation. These two terms sum to $3u_1u_2$. The first term of the corresponding negative contributions to the third harmonic is $3u_4u_1^*$. This term and its successors are neg-

ligible for all but the focal region of the highest intensity propagations considered here.

The harmonic sources of the second harmonic and third harmonic are thus $1u_1u_1$ and $3u_1u_2$, respectively. At a given point in the field of the propagating beam then, the finite amplitude production of the second harmonic is proportional to the square of the fundamental harmonic's amplitude. The production of the second harmonic off the beam axis is very small, since the amplitude of the fundamental beam there is quite small. The third harmonic is produced in proportion to the product of the first and second harmonics, and thus its nonlinear production is even more strongly weighted towards the beam axis.

Also of interest is how the production of the second and third harmonics varies with the z coordinate. Neglecting the effects of absorption and approximating the effects of focusing by assuming spherically-converging wave propagation, we should expect the amplitudes of the fundamental harmonic's mainbeam to increase linearly with distance from the source to the focus. At $z = F/2$, the on-axis amplitudes of the beam should be about twice the corresponding source plane amplitudes. Following from the same approximations, the fundamental's mainbeam width at $z = F/2$ should be about half its source plane width. Thus at $z = F/2$, the area of the fundamental's mainbeam should be about $1/4$ the corresponding source plane area. Together this relation and the previous amplitude relation suggest that the second harmonic beam production rate versus z is constant ($z < F$), with rate losses due to the diminishing fundamental mainbeam area balanced by the concurrent gains due to increased fundamental amplitudes. In spite of the gross approximations used in deriving this relation, initial computational analysis suggests that it is a useful approximation.

An analogous derivation for the relationship between z distance and the nonlinear production of the third harmonic will not be pursued here. The fact that the third harmonic production is proportional to the product of the fundamental and second harmonic amplitude, though, implies that the production of the third harmonic is strongly weighted towards the focal region. Fig. 7a displays the log-scaled, axial velocity amplitudes of the fundamental, second, and third harmonics. The source was the same focused 2 MHz Gaussian source considered in Section II.A. The medium's parameters were again those of liver. Consistent with the above observations, the amplitudes of the second harmonic exhibit a relatively large "gain" in its growth from low near field values to significant focal amplitudes. The third harmonic exhibits an even higher gain, roughly duplicating the growth in gain from the fundamental to second harmonic. Both harmonics, though, display post-focal region amplitude declines which parallel those of the fundamental.

Fig. 7b displays the corresponding log-scaled, focal plane ($z = 6$ cm) radial beam profiles. The fundamental profile drops 49.8 dB over the 1 cm radial range shown. The second harmonic roughly squares this decline in dropping 85.3 dB. The third harmonic then continues the relation-

ship in dropping 120.5 dB. These declines reflect the second and third harmonic, finite amplitude production rates discussed above. At $z = 8$ cm this relationship between the harmonic beam profiles continued to hold.

In Fig. 8 the axial amplitudes of the 4 MHz second harmonic beam are overlaid with those of the corresponding 4 MHz fundamental harmonic beam. The on-axis source intensity of both the respective propagations was 2 W/cm^2 . The axial curves have been normalized to be unity at $z = 6$ cm and log-scaled. The 4 MHz second harmonic focal amplitude was originally (pre-normalization) 15.0 dB below the corresponding 4 MHz fundamental value. The two curves are close through the focal region, then depart shortly after $z = 6$ cm as the 4 MHz linear curve rapidly declines.

The results displayed in Figs. 7 and 8 suggest that the 4 MHz second harmonic beam could be less susceptible to the defocusing effects of near field phase aberrations than a 4 MHz fundamental beam. Since only a fraction of the second harmonic beam forms in the near-field, only this fraction could be redirected or defocused by near-field jitter. The corresponding 2 MHz fundamental beam, though, would pass in its entirety through the aberration and suffer the consequent defocusing effects, including increased focal plane sidelobe levels. Secondly, these higher 2 MHz sidelobe levels could in turn increase the off-axis nonlinear production of the 4 MHz second harmonic. The next section will consider the effects of phase aberrations on linear and nonlinear harmonic beams. The potential of the nonlinear harmonics to improve on the inhomogeneous imaging performance of linear harmonics will depend on their ability to maintain lower sidelobe levels.

V. THE EFFECTS OF PHASE ABERRATING INHOMOGENEITIES ON LINEAR AND NONLINEAR BEAM PROPAGATIONS

In order to investigate the effects of tissue-based phase aberration on the characteristics of linear and nonlinear beams, planes of phase delay or jitter were introduced into linear and nonlinear propagations of the focused Gaussian transducer. These phase delay planes were computed using measured time delays from five abdominal wall layers [4] and five breast wall layers [7]. The five abdominal wall specimens had layer thicknesses of 2.5, 2.0, 1.5, 1.5, and 1.0–3.0 cm (a non-uniform layer), giving an average thickness of 1.9 cm. The five breast wall specimens had layer thicknesses of 1.5–2.5, 3.0–3.5, 3.5, 4.0, and 2.0–2.5 cm, giving an average thickness of 3.0 cm. The average thicknesses of the non-uniform layers were used to compute the five-layer averages. All of the abdominal wall and breast wall layers contained an outer skin layer.

Each of the measured abdominal wall time delay planes was converted to an equivalent 2 MHz phase delay plane. Each of these delay planes was then scaled by 0.5 (i.e., each phase delay was reduced by a factor of 2) and then applied twice to a given beam propagation to represent the cumulative aspect of the actual tissue delays. In ap-

plying a single delay plane, the 2 MHz phase delay values were scaled for appropriate application to each harmonic present in the computed field. The first delay plane was encountered by the propagating field at $z = 0.5$ cm and the second plane at $z = 1.5$ cm. Further, subdivision (and subsequent application) of the abdominal wall delay data did not appear to be necessary since it did not significantly change the resulting focal plane fields. Thus, it appeared that the 2 delay plane application scheme satisfied the thin lens approximation [26]. The breast delay planes were likewise applied in two steps, the first at $z = 1$ cm and the second at $z = 2$ cm. For both tissue types, the z placement was selected to represent the average slice thickness and also be convenient for the Δz step size utilized by the linear propagation.

Fig. 9 (a-f) depicts pairs of one-way focal plane harmonic amplitude diameters and the corresponding average radii for an unjittered (or homogeneous) path and an abdominal wall-jittered propagation path. The propagation parameters of both media were again those of liver. In Fig. 9a the corresponding focal plane diameters for the unjittered and jittered 2 MHz fields are overlaid. In Fig. 9b the corresponding average radii are shown for the 2 MHz fields. The average radii were obtained by averaging the focal plane grid of amplitudes around the axis. The corresponding results for the second harmonic 4 MHz and the fundamental 4 MHz fields are shown in Figs. 9(c-d) and 9(e-f), respectively.

In Fig. 9, two basic effects of jitter are visible. The first is the increased sidelobe levels associated with the defocusing of the abdominal wall phase delays. This sidelobe effect is more prominent for both of the 4 MHz fields than for the 2 MHz fundamental field. The shorter wavelengths of these 4 MHz fields allows for greater de-focusing by the phase screen. The second harmonic 4 MHz field also gets a sidelobe level increase from the corresponding increase in the 2 MHz field's sidelobe levels.

The second impact revealed in Fig. 9 is that there are small changes in the mainlobes of all three harmonic fields. In particular, in the diameter figures a shift in the peak or center of the jittered mainlobes can be seen. In the corresponding average figures, though, the impact of the jitter appears to be negligible, down to approximately 20 dB below the peak on-axis value. Thus, the impact of this abdominal wall-jittering doesn't appear to involve any significant broadening of these mainlobes. Finally, both of the jittered 4 MHz mainlobes show decreases in peak amplitudes which are consistent with the increased energy present in the sidelobe regions.

Fig. 10 shows two-way average radii results for the same abdominal wall-jittered propagations. Each of the curves shown was obtained by radially averaging the corresponding two-way planar data and then scaling the on-axis value to unity. The 2 MHz fundamental, 4 MHz second harmonic, and 6 MHz third harmonic average radii are shown in Fig. 10a. The 2, 4, and 6 MHz fundamentals are shown in Fig. 10b. The average two-way sidelobe levels of the second and third harmonic can be seen to be significantly

lower than those of any of the fundamental harmonics. In Fig. 10c, the two 4 MHz average two-way profiles are shown. The 4 MHz fundamental curve has a slightly narrower mainlobe (9.5% at 20 dB down from peak) and significantly higher sidelobe levels than the 4 MHz second harmonic profile. Likewise, Fig. 11(d) shows the 6 MHz fundamental and 6 MHz third harmonic two-way profiles. The 6 MHz fundamental curve is 10.9% narrower at the -20 dB level and also shows higher sidelobe levels than the third harmonic curve.

The results shown in Fig. 10 suggest that the second and third harmonics maintain lower sidelobe levels than the corresponding fundamental harmonics in propagating through abdominal wall. In Fig. 11, radial results obtained by averaging across five abdominal wall-jittered propagations are shown. In Fig. 11a depicts the normalized radial averages from the five two-way planar amplitude data sets. The average 2 MHz result is overlaid with the corresponding 4 MHz second harmonic and 4 MHz fundamental curves. The -20 dB width of the 4 MHz fundamental profile is 6.6% narrower than the 4 MHz second harmonic profile. The -20 dB width for this and subsequent multiple propagation-averaged results are given in Table III.

Each of the two-way average profiles shown in Fig. 11a was then radially summed. Each of the average profiles consisted of 499 radial position-magnitude value pairs, (r_i, m_i) , $i = 1, \dots, 499$. The 499 pairs discretely described the average of five abdominal wall-jittered, two-way profiles over a radial extent of 1.2 cm. The discrete radial summation of the average profiles was defined by 499 radial position-summation value (r_j, s_j) pairs, where each s_j was defined by $s_j = \pi \sum_{i=1}^j [(r_i^2 - r_{i-1}^2) \times (m_i + m_{i-1}) / 2]$. The first term in the summation involves the (r_0, m_0) on-axis magnitude value.

The resulting radial summation or integration profiles are shown in Fig. 11b. Each of these integrated two-way profiles was scaled such that the value at an off-axis radial distance of 1.2 cm was unity. The elevated sidelobes of the 2 and 4 MHz fundamental profiles cause their summation profiles to rise significantly beyond the radial extent of the mainlobe. This additional rise represents the potential for scattering from the sidelobes to significantly reduce the contrast resolution of the image. In Table III the radial extent at which these integration profiles reach the 0.9 level is given. This radial extent is a measure of the sidelobe's potential to reduce the contrast resolution of an image. In this case the second harmonic's radial extent is 38% less than that of its 2 MHz fundamental, and 63% less than the corresponding 4 MHz fundamental radial extent.

Alternatively, the summation profiles depicted in Fig. 11b offer the percent of the two-way field's amplitude inside or outside a given radius. For example, 91.7% of the 2 MHz fundamental's amplitude, 96.7% of the 4 MHz second harmonic's amplitude, and 88.6% of the 4 MHz fundamental's amplitude fall inside a radius of 0.25 cm. The corresponding percentages falling outside of 0.25 cm are 8.3%, 3.3%, and 11.4%, respectively. Ratios of these outside percentages could be useful for inferring the rela-

tive contrasts offered in imaging a low scattering or void region of a given size. For a void region approximately 0.5 cm across, the 4 MHz second harmonic of this device might then provide 2.5 times (8 dB) higher contrast than the 2 MHz fundamental, and 3.5 times (11 dB) higher contrast than the corresponding 4 MHz fundamental.

The previous two sets (at 2 and 4 MHz) of five abdominal wall-jittered propagations were repeated at twice the source frequencies. Fig. 12a-b depicts the corresponding averaged results from these 4 MHz nonlinear and 8 MHz linear propagations. In Fig. 12a the radial average amplitude curves obtained by averaging the five two-way data sets are shown. Note in Fig. 12a that the 8 MHz fundamental mainbeam is broader than the corresponding 4 MHz fundamental mainbeam. The jitter-imposed lateral resolution limits have been encountered, and in fact exceeded, at this point. Also note that the 8 MHz second harmonic mainbeam is narrower than either of the fundamentals'. Fig. 12b depicts the additional sidelobe corruption of the fundamental beams, and the corresponding increase in the second harmonic's relative contrast resolution potential.

Fig. 13a-b shows average results from five propagations through breast wall delay data. In Fig. 13 the results considered were from 2 MHz nonlinear and 4 MHz linear propagations. In Fig. 13a, the 4 MHz mainbeams are significantly broadened over the corresponding abdominal wall-jittered mainbeams in Fig. 11a. The sidelobe levels in Fig. 13a are also higher than those in Fig. 11a. As was observed in [7], the breast wall layers produced significantly more distortion than the abdominal wall layers. The second harmonic 4 MHz profile is 8.4% narrower at the -20 dB level than the fundamental 4 MHz. In Fig. 13b the integrated profile of the second harmonic has a radial extent at the 0.9 level, which is 48% less than the 2 MHz fundamental's and 70% less than the 4 MHz fundamental's. Thus, in the more distorting breast wall-jittered propagations, the relative advantages of the 4 MHz second harmonic were larger than in the abdominal wall propagations and included a slightly narrower mainbeam. The 4 and 8 MHz results for breast wall-jittered propagations followed closely the developments previously seen in the 4 and 8 MHz curves of Fig. 12a-b. Results from these propagations are included in Table III.

Finally, in all of the jittered propagations considered, the second harmonic mainbeam was narrower than the fundamental mainbeam. The limits on the lateral resolution of the linear harmonics though, eventually put limits on the second and other higher harmonics.

VI. DISCUSSION AND CONCLUSIONS

The previous sections showed the predicted liver-path beam patterns for a focused Gaussian-apodized transducer operating at 2, 4, and 8 MHz. The non-phase aberrated propagations suggested that the second and higher harmonics formed through finite amplitude distortion should have much lower sidelobe levels than their fundamental

harmonic or the corresponding linear fundamentals. The finite amplitude production of these higher harmonic beams should allow this sidelobe relationship to hold for any focused or unfocused transducer. Pulse propagation analysis suggested that the higher harmonics formed in a propagating pulse-beam can be very well described by considering the harmonics produced in the corresponding continuous wave propagation. Modeling results also predicted that second harmonic levels sufficient for imaging purposes could be obtained within the field amplitude limits of the mechanical index.

The introduction of phase jitter as computed from measured propagation delays from slices of abdominal wall and breast wall caused the sidelobe levels of the second harmonic and fundamental beams to rise significantly. In all the aberrated propagations considered, the two-way profile of the second harmonic offered narrower -20 dB mainlobe widths and lower sidelobe levels than the fundamental beam which produced it. These same second harmonic profiles had slightly broader mainlobes at 4 MHz in abdominal wall-jittered propagations than the 4 MHz fundamental profiles. In all other jittered propagations considered, the second harmonic offered slightly narrower mainlobes than the same-frequency fundamental, and substantially lower sidelobe levels. Thus, it appears that second harmonic-based ultrasonic images could offer significant improvement in the lateral component of contrast resolution.

One obstacle to obtaining such images would be artifacts from source contributions to the higher harmonic bandwidths. Such artifacts are evident, for example, in measured pulses [27]. Perhaps it would not be possible to produce source waves with as little energy content outside the main bandwidth as that depicted in Fig. 5.

Fig. 14a depicts such an imperfect source wave. This on-axis waveform is depicted in particle velocity units and corresponds to a peak pressure of one half of that of the pulse shown in Fig. 5a. The pulse in Fig. 14a has the same form as that in Fig. 5a, with the exception of the initial zero portion. Fig. 14b shows the corresponding source pulse spectrum. Significant energy content outside the 2 MHz bandwidth is visible. The resulting computed focal waveform's spectrum is depicted in Fig. 14c and can be compared to the earlier focal spectrum in Fig. 5b. Considering the log-scaled depiction in Fig. 14c, it is apparent that a simple high pass filtering of the received spectrum would contain significant contributions from the source.

Fig. 14(d) shows the resulting nonlinear distortion pulse obtained by high-pass filtering the spectrum of Fig. 14c. This pulse can be compared to the corresponding distortion pulse shown in Fig. 5c. In both cases the cut-off frequency was 3 MHz. In Fig. 14(d) the full 8 microsecond period of the computed pulse is shown so that the ringing associated with the linear or source content within the second harmonic bandwidth can be seen. This ringing could substantially hurt the axial component of the contrast resolution and might negate the lateral gains associated with the lower sidelobe levels. In this case, improvement could be obtained by increasing the source amplitude so as

TABLE III

-20 dB FULL-WIDTHS FOR THE AVERAGE TWO-WAY PROFILES SHOWN IN 11A, 12A, AND 13A. FULL-WIDTHS AT THE 0.9 LEVEL FOR THE INTEGRATED PROFILES OF 11B, 12B, AND 13B. ALSO INCLUDED ARE THE RESULTS FROM THE 4 MHz NONLINEAR AND 8 MHz LINEAR BREAST WALL-JITTERED PROPAGATIONS (WHICH WERE NOT SHOWN IN FIGURE FORM). NOTE THE MISERABLE RESULTS GIVEN FOR THE 8 MHz FUNDAMENTAL BREAST WALL-JITTERED PROPAGATIONS.

Frequency/Medium	-20 dB full-width (cm)	0.9 Integrated full-width (cm)
2 MHz/ab wall	0.388	0.458
4 MHz/ab wall	0.242	0.542
2nd har 4 MHz/ab wall	0.258	0.332
8 MHz/ab wall	0.304	0.602
2nd har 8 MHz/ab wall	0.216	0.338
2 MHz/br wall	0.406	0.746
4 MHz/br wall	0.334	0.858
2nd har 4 MHz/br wall	0.308	0.504
8 MHz/br wall	0.462	0.880
2nd har 8 MHz/br wall	0.298	0.526

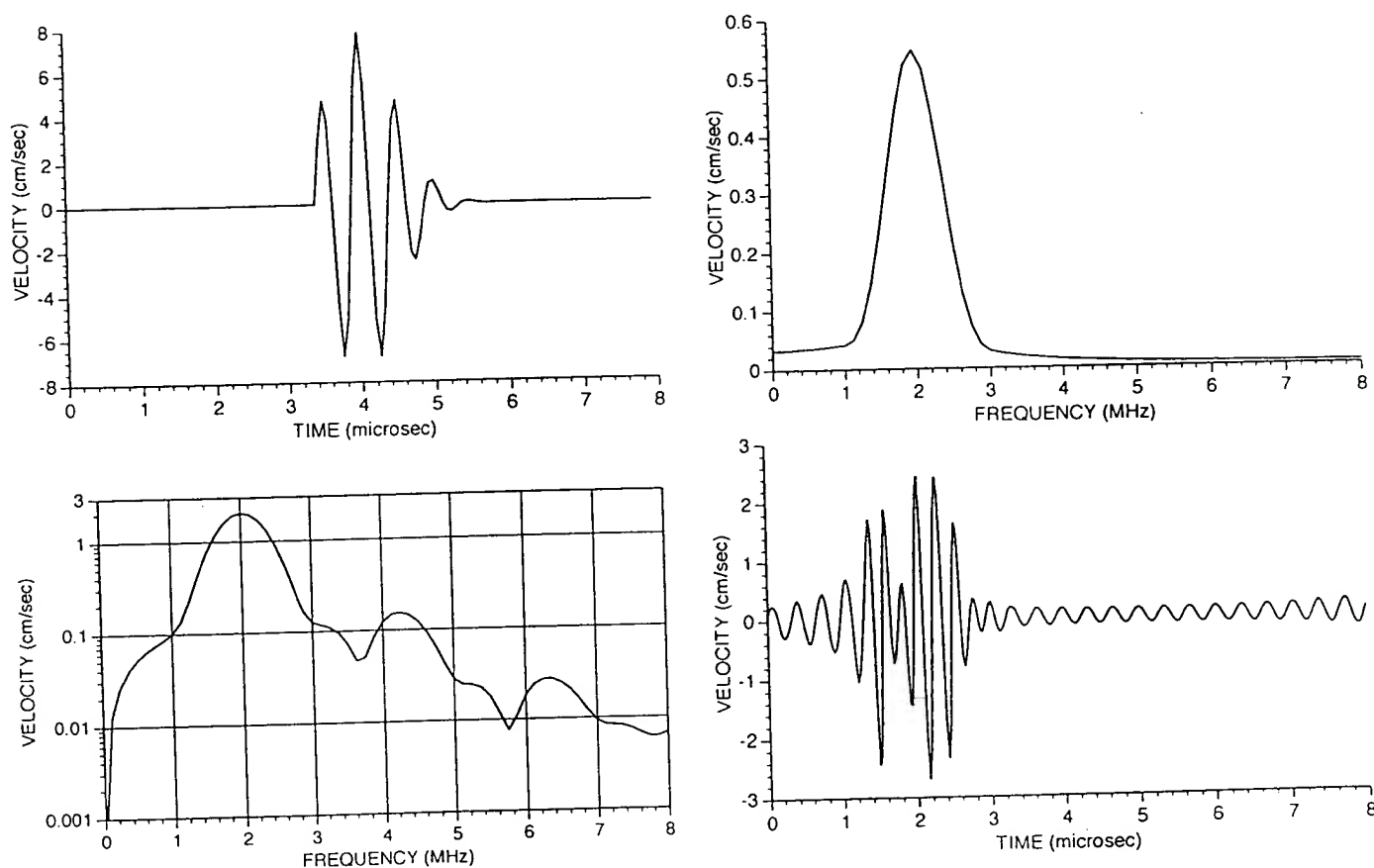


Fig. 14. (a) An imperfect (on-axis) source pulse. (b) The corresponding spectrum. (c) The log-scaled, un-jittered focal spectrum. (d) The corresponding nonlinear distortion pulse obtained by constructing with the spectral information in (c) starting at 3 MHz.

to boost the second harmonic bandwidth levels. Such an amplitude-dependent strategy might not be desirable, and is further complicated by the fact that off-axis the second harmonic drops off much faster than the source content in the same bandwidth.

In order to eliminate such problems, a two-pulse scheme appears to be a good solution. In this method, two source pulses would be sent in place of a single pulse in the image formation cycle. The two pulses would be identical in form,

but one would be significantly lower in amplitude. The received echo from this lower amplitude pulse could then be used to remove the linear content from the high amplitude pulse. This could be accomplished by subtracting an appropriately-scaled version of the received low amplitude signal from the corresponding high amplitude signal. The resulting difference signal should then be high-pass filtered, followed by the normal sequence of image formation steps. The high-pass filtering would be necessary here since

pulse analysis has revealed that the low frequency content of the difference signal is radially wide-spread and could greatly reduce the higher harmonic sidelobe advantage.

Fig. 15 shows results relevant to an implementation of the two-pulse scheme using the pulse shown in Fig. 14a as the high amplitude source pulse. In Fig. 15a, the focal spectrum from 14c is overlaid with the focal spectrum produced by a half-amplitude version of the same source. The low or half-amplitude spectrum was multiplied by two and subtracted from the high amplitude spectrum to obtain the difference spectrum depicted in Fig. 15b. Note that if the propagations had not involved finite amplitude distortion, then this difference spectrum would have been all zero. The difference spectrum was then high-pass filtered and inverse transformed to obtain the effective on-axis distortion imaging pulse shown in Fig. 15c. Compare this pulse with that shown in Fig. 14(d). The transition for the high-pass filtering was at 2.75 MHz. This same frequency was also appropriate for filtering off-axis difference spectra.

Initial analysis suggests that this two-pulse scheme appears to be capable of extracting the desired largely-second harmonic images from any realistic ultrasonic imaging pulse. The third harmonic bandwidth depicted in Fig. 15b though, does not appear to be separable from the second harmonic bandwidth. The nodal depth between these harmonics is not deep enough. Thus, third harmonic (or largely-third harmonic) images do not appear to be obtainable with this two pulse scheme. Unless source pulses can be produced with very little energy outside the main bandwidth (see the spectrum in Fig. 5b), the production of third harmonic images might not be constructive in light of axial resolution problems. Initial analysis also suggest that a two pulse imaging scheme with a $1/4000$ second interval between the respective high and low amplitude source pulses, should not have significant artifacts due to tissue or transducer motion.

The use of the second harmonic (plus a little contribution from higher harmonics) to form an image is an independent alternative to the phase correction-based schemes which have been and are being examined by other investigators as a means for improving the contrast performance of biomedical ultrasonic imaging. If one or more of these phase or beam correction schemes proves successful, then they could also be used to improve the contrast of nonlinear images. To the extent that a phase correction method improves the *in vivo* focusing of a beam it should decrease the beam's sidelobe levels. The corresponding sidelobe level decrease for the constituent finite amplitude harmonics should be larger than for the fundamental.

The higher harmonics may also offer some additional opportunities for correcting for beam distortion. The amplitude of the third harmonic in the focal region is strongly affected by the fundamental's amplitude. As discussed in Section IV, the nonlinear production of the third harmonic is proportional to the product of the amplitudes of the fundamental and second harmonics. This means that much of the third harmonic's production occurs in the focal region where beam distortion can significantly reduce the am-

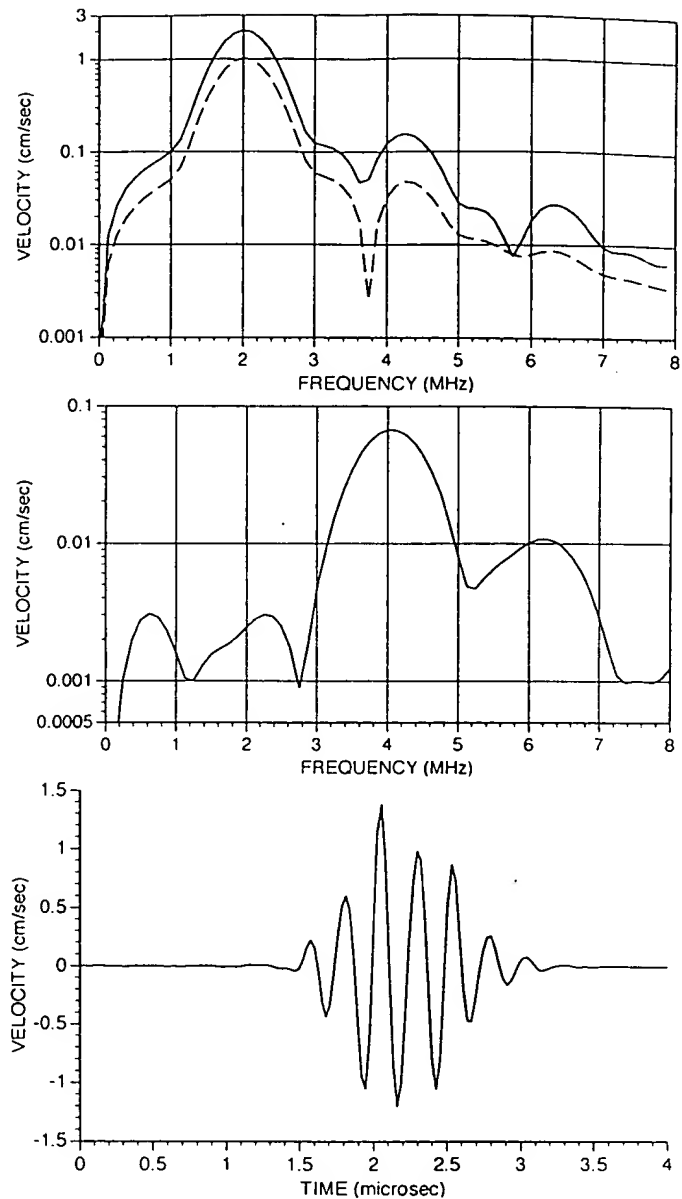


Fig. 15. The log-scaled focal spectrum from 14c overlaid with the focal spectrum from the same source using a half amplitude version of the source pulse (as depicted in Fig. 14a). (b) The resulting difference spectrum computed for the two spectra shown in (a). (c) The corresponding nonlinear distortion pulse obtained by constructing with the spectral information in (b) starting at 2.75 MHz.

plitude of the fundamental and second harmonic. It thus might be possible to develop an iterative scheme to correct for beam defocusing, using the amplitude of the received third harmonic for feedback.

Second harmonic images may also provide for a means of reducing speckle. In particular, an image formed as the sum of a second harmonic image and the corresponding fundamental image should have less speckle than either of the constituent images. Since the second harmonic is twice the frequency of the fundamental and has a largely constant phase relationship with the fundamental in the main-lobe, the second harmonic image's speckle pattern should be conveniently out of phase with that of the fundamental.

Finally, statistically-defined jitter planes were also used (as an alternative to phase delay planes directly computed from measured temporal delays). Using the RMS temporal fluctuation and spatial correlation lengths computed for the abdominal wall [4] and breast wall [7] measurements and the algorithms given in [28], jitter planes were computed. Unfortunately, these simulated jitter planes gave markedly different defocusing results than the measured delay planes, so they were abandoned.

The results of this study suggest that the finite amplitude distortion of biomedical ultrasonic imaging pulses could be utilized to enhance the contrast resolution of images. Experimental work is planned. Additionally, other uses for finite amplitude distortion may be possible as well.

ACKNOWLEDGMENTS

Helpful discussions with E. L. Carstensen, X. Chen, L. M. Hinkleman, K. N. Kumar, D. L. Liu, T. D. Mast, K. J. Parker, and R. C. Waag are gratefully acknowledged. The efforts of L. M. Hinkleman and D. L. Liu to provide the measured tissue delay data were invaluable.

REFERENCES

- [1] M. Moshfeghi and R. C. Waag, "In vivo and in vitro ultrasound beam distortion measurements of a large aperture and a conventional aperture focused transducer," *Ultrasound in Med. and Biol.*, vol. 14, pp. 415-428, 1988.
- [2] L. Nock and G. E. Trahey, "Phase aberration correction in medical ultrasound using speckle brightness as a quality factor," *J. Acoust. Soc. Am.*, vol. 85, pp. 1819-1833, 1989.
- [3] S.H.P. Bly, D. Lee-Chahal, D. R. Foster, M. S. Patterson, F. S. Foster, and J. W. Hunt, "Quantitative contrast measurements in B-mode images: comparison between experiment and theory," *Ultrasound in Med. and Biol.*, vol. 12, pp. 197-208, 1986.
- [4] L. M. Hinkleman, D. L. Liu, L. A. Metlay, and R. C. Waag, "Measurements of ultrasonic pulse arrival time and energy level variations produced by propagation through abdominal wall," *J. Acoust. Soc. Am.*, vol. 95, pp. 530-541, 1994.
- [5] D. L. Liu and R. C. Waag, "Time-shift compensation of ultrasonic pulse focus degradation using least-mean-square estimates of arrival time," *J. Acoust. Soc. Am.*, vol. 95, pp. 542-555, 1994.
- [6] D. L. Liu and R. C. Waag, "Correction of ultrasonic wavefront distortion using back propagation and a reference waveform method for time-shift compensation," *J. Acoust. Soc. Am.*, vol. 96, pp. 649-660, 1994.
- [7] L. M. Hinkleman, D. L. Liu, L. A. Metlay, and R. C. Waag, "Measurements of ultrasonic pulse arrival time and energy level variations produced by propagation through breast wall," *J. Acoust. Soc. Am.*, vol. 95, pp. 530-541, 1994.
- [8] R. Mallart and M. Fink, "Adaptive focusing in scattering media through sound speed inhomogeneities: The van Cittert Zernicke approach and focusing criterion," *J. Acoust. Soc. Am.*, vol. 96, pp. 3721-3732, 1994.
- [9] Q. Zhu and B. D. Steinberg, "Wavefront amplitude distribution in the female breast," *J. Acoust. Soc. Am.*, vol. 96, pp. 1-9, 1994.
- [10] Q. Zhu and B. D. Steinberg, "Wavefront amplitude distortion and image sidelobe levels: Part I - Theory and computer simulations," *IEEE Trans. Ultrason. Ferroelec. Freq. Contr.*, vol. 40, pp. 747-753, 1993.
- [11] Q. Zhu and B. D. Steinberg, "Wavefront amplitude distortion and image sidelobe levels: Part II - In vivo experiments," *IEEE Trans. Ultrason. Ferroelec. Freq. Contr.*, vol. 40, pp. 747-753, 1993.
- [12] J. Y. Lu, H. Zou, and J. F. Greenleaf, "Biomedical ultrasound beam forming," *Ultrasound in Med. and Biol.*, vol. 20, pp. 403-428, 1994.
- [13] M. Karaman, A. Atalar, H. Koymen, and M. O'Donnell, "A phase aberration correction method for ultrasound imaging," *IEEE Trans. Ultrason. Ferroelec. Freq. Contr.*, vol. 40, pp. 275-288, 1993.
- [14] J. A. TenCate, "An experimental investigation of the nonlinear pressure field produced by a plane circular piston," *J. Acoust. Soc. Am.*, vol. 94, pp. 1084-1089, 1993.
- [15] A. C. Baker, K. Anastasiadis, and V. F. Humphrey, "The nonlinear pressure field of a plane circular piston: theory and experiment," *J. Acoust. Soc. Am.*, vol. 78, pp. 1483-1487, 1988.
- [16] P. T. Christopher and K. J. Parker, "New approaches to nonlinear diffractive field propagation," *J. Acoust. Soc. Am.*, vol. 90, pp. 488-499, 1991.
- [17] M. A. Averkiou and M. F. Hamilton, "Measurements of harmonic generation in a focused finite-amplitude sound beam," *J. Acoust. Soc. Am.*, vol. 98, pp. 3439-3442, 1995.
- [18] T. Christopher, "Modeling acoustic field propagation for medical devices," Ph.D. thesis, U. of Rochester, 1993.
- [19] T. Kamakura, M. Tani, Y. Kumamoto, and K. Ueda, "Harmonic generation in finite amplitude sound beams from a rectangular aperture source," *J. Acoust. Soc. Am.*, vol. 91, pp. 3144-3151, 1992.
- [20] A. C. Baker, A. M. Berg, A. Sahin, J. N. Tjøtta, "The nonlinear pressure field of plane, rectangular apertures: Experimental and theoretical results," *J. Acoust. Soc. Am.*, vol. 97, pp. 3510-3517, 1995.
- [21] M. E. Lyons and K. J. Parker, "Absorption and attenuation in soft tissues II - experimental results," *IEEE Trans. Ultrason. Ferroelec. Freq. Contr.*, vol. 35, pp. 511-521, 1988.
- [22] S. A. Goss, R. L. Johnston, and F. Dunn, "Compilation of empirical ultrasonic properties of mammalian tissues. II," *J. Acoust. Soc. Am.*, vol. 68, pp. 93-108, 1980.
- [23] W. K. Law, L. A. Frizzell, and F. Dunn, "Determination of the nonlinearity parameter B/A of biological media," *Ultrasound in Med. and Biol.*, vol. 11, pp. 307-318, 1985.
- [24] P. T. Christopher, "A nonlinear plane wave algorithm for diffractive propagation involving shock waves," *J. Comp. Acoust.*, vol. 1, pp. 371-393, 1993.
- [25] T. Christopher, "Modeling the Dornier HM3 lithotripter," *J. Acoust. Soc. Am.*, pp. 3088-3095, 1994.
- [26] J. W. Goodman, *Introduction to Fourier Optics*. New York: McGraw-Hill, 1968.
- [27] A. C. Baker and V. F. Humphrey, "Distortion and high-frequency generation due to nonlinear propagation of short ultrasonic pulses from a plane circular piston," *J. Acoust. Soc. Am.*, pp. 1699-1705, 1992.
- [28] D. L. Knepp, "Multiple phase-screen calculation of the temporal behavior of stochastic waves," *Proceedings of the IEEE* 71(6), pp. 722-737, 1983.

Ted Christopher was born in Baltimore, Maryland in 1960. He received the B.S. degree in Computer and Information Science from the University of Massachusetts, Amherst, MA in 1981 and the M.S. and Ph.D. degrees in Electrical Engineering from the University of Rochester, Rochester, NY in 1984 and 1993, respectively. He is currently working at the Diagnostic Ultrasound Research Laboratory at the University of Rochester. He has held a number of ultrasound research and teaching-related positions at the University of Rochester over the last 12 years. His research interests include modelling biomedical ultrasonic wave propagation and improving the quality of biomedical ultrasonic images.

Evidentiary Declaration of Sharon Mulvagh, M.D.

RECEIVED
MAR 29 98
GROUP 330

I, Sharon L. Mulvagh, M.D., declare that I believe the following facts to be correct based on my personal knowledge:

1. I am a medical doctor on staff at the Mayo Medical Clinic, and have held this position since November 1989.
2. I made a presentation to a number of medical colleagues on or about September 30, 1994, in the Knickerbocker Hotel in Chicago, Illinois, at an echocardiography conference entitled "Advances in Echocardiography: Contrast Echocardiography Perfusion Imaging." My presentation was part of Session I of the day. The Session was entitled, "New Agents: Experimental and Clinical Studies, New Technologies."
3. My presentation included a videotape showing the Imagent® contrast agent on an Acuson 128 machine. The tape is identified by Mayo Clinic ID# CSI, and Echo Date 9-28-94. The machine was configured to transmit ultrasound energy at a fundamental frequency (2.5MHz), and receive ultrasound echoes from the anatomy and/or contrast agent at a harmonic (5MHz) of that frequency. This configuration is indicated by the highlighted 5.0MHz icon on the video images.
4. The videotape I presented showed images of a dog's beating heart, in the absence of contrast agent (called "Baseline Imagent" on the tape), as well as images with contrast agent subsequently injected into the dog. Accordingly, harmonic images of the tissue were seen, followed by harmonic images of the contrast agent. The 8/22/94 date on the videotape represents the date on which the taped experiment was conducted.
5. I have enclosed two videotapes. The first videotape is a partial copy of portions of the videotape I presented and has a thin crack in the right-hand window. The second videotape is a complete copy of the videotape I presented and is marked "Mayo Clinic #CSI, Echo Date 9-28-94, Complete Copy".
6. The conference presentation was open to all who attended, with no obligations of confidentiality on the part of the attendees. Accordingly, I considered my disclosure to be public.

I hereby declare under penalty of perjury that the foregoing is, to the best of my knowledge, correct.

Dated this 19th day of March, 1998, by Sharon L. Mulvagh
Sharon L. Mulvagh, M.D.

Evidentiary Declaration of Gregory L. Holley

I, Gregory L. Holley, declare that I believe the following facts to be correct based on my personal knowledge:

1. I am an Image Analysis Engineer at Acuson Corporation, and have held this position since July 20, 1987. I have been involved in the development of contrast imaging and second harmonic imaging at Acuson for the last several years.
2. I have reviewed the videotape referred to in the Declaration of Sharon L. Mulvagh, M.D.
3. The videotape shows that the Acuson 128 system was transmitting ultrasound energy into a dog's beating heart at a fundamental frequency and receiving ultrasound echoes at a harmonic frequency, irrespective of whether or not contrast agent had been injected into the dog.
4. The tape shows harmonic imaging, in the absence of contrast agent, in the section entitled "Baseline Imagent". During this part of the imaging, a second harmonic image of the tissue of the dog's heart is shown. For approximately the first eight seconds of this image, no contrast agent is visible in the image. The image that is visible is formed at least in part from the second harmonic response of the tissue to the transmitted ultrasound wave. The image is not formed from harmonic scattering by a contrast agent.
5. I have reviewed the paper by Ted Christopher entitled, "Finite Amplitude Distortion-Based Inhomogeneous Pulse Echo Ultrasonic Imaging," (IEEE Trans. USFC 44(1) (Jan. 97) pp. 125-139). Finite amplitude distortion during the propagation of the ultrasound wave through the body, as described in Christopher's paper, is the mechanism by which the second harmonic response of the tissue is generated. This response contributes to the displayed image of the dog's heart that is based upon echoes received at the harmonic frequency.
6. I also reviewed the videotape entitled "Contrast Echocardiography Investigations," referred to in paragraph 13 of Joan C. Main's declaration.
7. In a segment of this videotape entitled "Experiment 1", a video clip is shown on the right side of the screen labeled "Second harmonic with contrast." This video clip shows a short axis view of an animal's heart. The first second or so of this clip shows a second harmonic image of the animal's heart in the absence of contrast agent. The display shows a second harmonic image of the tissues of the heart itself. This image derives at least in part from second harmonic distortion that occurs as the transmitted ultrasound pulse propagates through the tissues of the animal subject. In my opinion, such second harmonic distortion makes a measurable contribution to these images. As noted in paragraph 5, "finite amplitude distortion" is a name for the mechanism by which this second harmonic distortion is generated.
8. Another example of images formed in part from second harmonic generated by finite amplitude distortion is shown in the segment labeled "Experiment 2." Again, the right side of the screen shows a second harmonic video clip. For at least the first several frames, there

RECEIVED
MAR 20 98
GROUP: 330

is no contrast agent visible in the left ventricle of the heart (the image is oriented so the left ventricle is visible on the right side of the video clip). In these first several frames, the image of the tissues of the left ventricle seen in the clip is formed at least in part from second harmonic distortion of the transmitted pulse caused by propagation through the tissues of the animal, and not from second harmonic scattering from the contrast agent. In my opinion, such second harmonic distortion makes a measurable contribution to the images in these first several frames.

I hereby declare under penalty of perjury that the foregoing is true and correct.

Dated this 18th day of March, 1998, by Gregory L. Holley
Gregory L. Holley

Evidentiary Declaration of Joan C. Main

I, Joan C. Main, declare that I believe the following facts to be correct based on my personal knowledge:

1. I have been employed in the marketing department of Acuson Corporation since May 1986. My primary focus over the last few years has been in the area of contrast imaging. In connection with my responsibilities in this area, I have worked closely with physicians having a research interest in the field.
2. I also worked with an Acuson engineer, Paul Chandler, in supporting second harmonic engineering development efforts. He made modifications to our Acuson 128 ultrasound system to support transmission at a fundamental center frequency of 2.5MHz and reception at a harmonic center frequency of 5.0MHz. Special wideband transducers were developed for these investigations by Acuson's Principal Fellow, Amin Hanafy.
3. Among the initial physicians with whom I worked were Doctors Sharon Mulvagh and Tony DeMaria. In working with these physicians, I assisted in the operation of the modified Acuson 128 system, which is internally known and labeled as System 1122.
4. Specifically, in working with Doctor Sharon Mulvagh in August 1994, I brought Acuson's System 1122 to the Mayo Clinic to do dog studies with the Imagent® contrast agent from Alliance Corporation in San Diego. We videotaped the dog's beating heart while imaging with System 1122, in the harmonic mode. Baseline images were gathered first. Then contrast agent was injected into the dog's vein, and contrast images were gathered. I personally did at least some of the imaging for this study.
5. Segments from this study were shown in a presentation that Dr. Mulvagh made and that I attended, on or about September 30, 1994, in the Knickerbocker Hotel in Chicago, Illinois, at an echocardiography conference entitled "Advances in Echocardiography: Contrast Echocardiography Perfusion Imaging Transesophageal Echo." Her presentation was part of Session I of the day. The Session was entitled, "New Agents: Experimental and Clinical Studies, New Technologies."
6. Her presentation included a videotape showing the use of the contrast agent Imagent® on an Acuson 128 machine. Images on this tape came from the study that we worked on together. The tape is identified by Mayo Clinic ID#CSI, and Echo Date 9-28-94. The machine was configured to transmit ultrasound energy at a fundamental frequency (2.5MHz), and receive ultrasound echoes from the anatomy and/or contrast agent at a harmonic (5MHz) of that frequency. This configuration is indicated by the highlighted 5.0MHz icon on the video images.
7. The videotape that she presented showed images of a dog's beating heart, taken on 8/22/94, both in the absence of contrast agent (called "Baseline Imagent" on the tape), as well as with contrast agent subsequently injected into the dog. In her presentation, she pointed out the baseline image prior to the contrast injection. Accordingly,

RECEIVED
MAR 20 98
CIVIL: 330

harmonic images of the tissue were seen, followed by harmonic images of the contrast agent.

8. The conference presentation was open to all who attended, with no obligations of confidentiality on the part of the attendees.
9. Turning now to my earlier work with Dr. DeMaria, in early 1993 I accompanied Paul Chandler and his clinical marketing team to conduct a proof of principle experiment. We did a pig and a dog study using System 1122 at the University of California at San Diego, with the Schering contrast agent called SSH508 (now known as Levovist®).
10. The studies were documented on Betacam videotape, and segments were chosen and edited for a private showing to Acuson's key luminaries worldwide. Paul Chandler and I presented the information on the tape to this group of physicians under a non-disclosure agreement on Sunday, March 14, 1993, prior to the start of the American College of Cardiology meeting in Anaheim, California.
11. On June 7, 1993, I sent the tape to TVA Incorporated in Mountain View to be converted to Super-VHS format for additional presentations to physicians and their staff.
12. Later in June of 1993, I personally presented the Betacam version of the videotape to key investigators on the show floor at the American Society of Echocardiography. This was a public showing, in that no non-disclosure agreements were signed or requested.
13. Enclosed is the Super-VHS version of the same videotape. It has the same images as were on the Betacam version that I presented at the American Society of Echocardiography.
14. This tape showed two experiments. In experiment number one, on the right side of the screen is a short axis view of an animal heart. For the first second or so of this video clip, there is no contrast agent present; the display just shows a harmonic image of the tissues of the heart itself.
15. The second experiment shows an apical 4-chamber view showing a second harmonic image of the heart while contrast agent is injected. For the first few frames, there is no contrast agent present in the left ventricle of the heart (on the right side of the image). The image of the left ventricle of the heart is formed at least in part from the second harmonic response of the tissue itself and not from a contrast agent.

I hereby declare under penalty of perjury that the foregoing is, to the best of my knowledge, correct.

Dated this 11 day of February 1998, by Joan C. Main
Joan C. Main, Marketing Manager